Algal Research 99 (2026) 104955

Contents lists available at ScienceDirect

Algal Research

journal homepage: www.elsevier.com/locate/algal

Chlorella vulgaris cultivation under super high light intensity: A tentative photobioreactor design

Victor Pozzobon

Université Paris-Saclay, CentraleSupélec, Laboratoire de Génie des Procédés et Matériaux, Centre Européen de Biotechnologie et de Bioéconomie (CEBB), 3 rue des Rouges Terres, 51110 Pomacle, France

ARTICLE INFO

Keywords:
Microalgae
Super high light
CFD
Design
Flashing light effect

ABSTRACT

In a previous article, *Chlorella vulgaris* was shown to grow under super high light (7 000 μmolPhotonPAR/m^2/s), if adequate light/dark patterns were used. However, this proof-of-concept was delivered in a 125-mL photobioreactor. This article is the first step towards upscaling the process to a lab-scale prototype (5-10 liters). A numerical workflow based on Computational Fluid Dynamics (Euler–Lagrange combined with Conjugate Heat Transfer) was implemented using the open-source toolbox OpenFOAM. After numerical validation of the workflow and discussion of the effects of Lagrangian Coherent Structures, the tool was applied to assess the performance of a 50x40x5 cm^3 baffled flat-panel photobioreactor. Light/dark patterns analysis demonstrated that their median frequency and duty cycle were too widely distributed to be considered actually controlled (0.510 ± 0.271 Hz and 0.460 ± 0.211, respectively). Also, Conjugate Heat Transfer simulations showed that the system components were relatively homogeneous thermally, opening the way to a thermal circuit modeling approach. To improve the design, a deflector tube was inserted between the baffles to channel the fluid flow. This enhancement allowed narrowing down the light/dark patterns features satisfactorily (0.625 ± 0.131 Hz and 0.271 ± 0.061 for the frequency and duty cycle, respectively). Variations in the design allowed for the demonstration of the modularity of the possible light/dark cycles (a 0.322 to 0.625 Hz frequency and a duty cycle between 0.200 and 0.430). Finally, thermal analysis suggests that such a prototype could operate safely, *i.e.*, with a culture medium temperature below 30 °C, under 20 000 μmolPhotonPAR/m^2/s.

1. Introduction

Since the middle of the twentieth century, photoautotrophic microalgae have attracted growing interest from both scholars and engineers [1]. Their appeal stems from their ability to simultaneously address nutritional, environmental, and industrial challenges. Indeed, microalgae can produce high-quality food and feed ingredients [2], as well as high-value bio-based compounds [3,4]. In parallel, they provide several environmental services, including carbon dioxide cycling, remediation of nitrogen- and phosphorus-polluted waters [5,6], and the potential valorization of residual biomass into biofuels [7]. This broad range of applications is particularly relevant in the current global context, where human activities continue to exert unsustainable pressure on natural resources, including fossil resources, freshwater, arable land, and biodiversity [8]. At the same time, modern Western lifestyles, characterized by reduced physical activity and consumption of ultra-processed foods, are associated with an increasing prevalence of metabolic disorders collectively referred to as metabolic syndrome [9], which could potentially be alleviated, at least in part, through dietary microalgae supplementation.

Still, among the reasons preventing microalgae from delivering on their promises is the fact that the biomass yields obtained from photoautotrophic microalgae cultivation remain low. This limitation largely arises from the dilute nature of light supply, which imposes an energetic limitation on the production process. In response to this bottleneck, several authors have developed next-generation photobioreactors and supporting concepts, such as optimized light-harvesting geometries [10], thin and ultra-thin bubble columns [11,12], thin-film and ultra-thin-film cascade photobioreactors [13,14], as well as light dilution (*e.g.*, DiCoFluV) and luminostat concepts [15,16]. While these initiatives have significantly advanced the field, they have explored only one of the two possible strategies for overcoming the energetic limitation that the production process is facing: maximizing the use of available light. The present work investigates an alternative paradigm, far less represented in the literature: dramatically increasing the light supplied to microalgae cultures.

There are, however, valid reasons why such an approach has received limited attention. First, it is commonly accepted that relatively low light intensities are sufficient to sustain maximal growth

E-mail address: victor.pozzobon@centralesupelec.fr.

https://doi.org/10.1016/j.algal.2026.104955
Received 2 July 2026; Received in revised form 24 August 2026; Accepted 8 September 2026
Available online 17 September 2026

(100 to 200 μmolPhotonPAR/m^2/s) [17–19]. Second, intense illumination is known to damage cells: 500 μmolPhotonPAR/m^2/s is already regarded as *high* [20], while 1300 μmolPhotonPAR/m^2/s is considered *excessive* [21]. Indeed, carelessly overpowering photosynthesis can lead to PSII damage [22,23], ultimately impairing the photosynthetic energy-harvesting process.

In addition, until recently, only three studies suggested that cultivation under super high light was feasible. These studies were conducted on well-stirred, optically dense cultures exposed to 3000, 7000, and 8000 μmolPhotonPAR/m^2/s, respectively [24–26]. In these cases, the combination of the light gradient inside the culture and the constant mixing supposedly induced an adequate perceived light pattern allowing the cells to grow. Consequently, experiments under optically thin conditions were needed to confirm that the observed growth originated from intrinsic biological mechanisms rather than solely from reactor-scale light heterogeneity. A proof-of-concept using *Chlorella vulgaris* was therefore established in 6-mm flat-panel photobioreactors operated in turbidostat mode to ensure that all growth occurred under the target illumination of 7000 μmolPhotonPAR/m^2/s [27]. The study demonstrated that, while continuous illumination completely inhibited proliferation, cycling light at frequencies between 0.1 and 100 Hz (square signal, duty cycle 0.5) enabled cells to proliferate at their nominal growth rate (approximately 2 day^{-1}).

The author proposed an explanation based on the flashing light effect. This concept originates from the pioneering work of Kok and Myers [28,29]. In essence, the flashing light effect consists of manipulating light delivery through alternating light and dark periods at frequencies unlikely to occur naturally (1 to 100 Hz) [30,31]. During the illuminated phase, cells capture light energy and store it in pools of energy-rich molecules. This phase must be sufficiently long to charge these pools, yet short enough to avoid their saturation and the generation of Reactive Oxygen Species (ROS). During the dark phase, cells use the stored energy to convert CO_2 into carbohydrate precursors (G3P). This phase must be long enough to process the stored energy carriers, while remaining short enough to prevent the cell from becoming idle. It was long hypothesized that, under certain conditions, this mechanism could increase the efficiency of the photosynthetic apparatus.

While much debated, several studies support its existence and have helped untangle the complex interplay between frequency, light intensity, and duty cycle. Among these parameters, frequency is arguably the best understood. Most authors agree that frequencies below 0.1 Hz (10 s cycle time) generally reduce growth because of increased dark respiration [32–35]. Conversely, frequencies above 1000 Hz yield results equivalent to continuous illumination at the same average intensity, as cells can no longer perceive the rapid oscillations [36]. The effects of the other parameters are more difficult to isolate. Nevertheless, several authors demonstrated that duty cycle exerts a non-linear effect modulated by cycle frequency [33]. Light intensity further complicates the picture. For example, studies performed at 5 Hz under high illumination (above 500 μmolPhotonPAR/m^2/s) showed that decreasing the duty cycle from 0.5 to 0.1 enhances photosynthetic oxygen production [36–38], whereas the opposite trend is observed under low illumination [36]. Beyond experimental observations, modeling studies also support the theoretical basis of the phenomenon [39,40]. Finally, very recent investigations have begun to unravel the subtle mechanisms occurring at the electron transport chain level [41], suggesting that tolerance to extremely high light intensities may be widespread, at least within the *Chlorella* genus.

Despite these promising results, obtained at a small scale, several questions remain regarding the feasibility of a super-high-light cultivation prototype (5–10 l) that would allow driving the experimental investigations further. Although building such a prototype would constitute a direct validation route, securing funding for such systems has proven quite difficult in the author's experience. While the biological concept itself appeared bold a few years ago, its upscaling still appears equally ambitious today. Addressing this challenge by proposing a numerical design showing the realizability of such a photobioreactor is therefore the objective of the present article. Three key questions must be answered. First, can a photobioreactor designed to handle super high light loads also ensure adequate cell cycling so that the flashing light effect remains operative? Second, because super-high-light cultivation involves substantial energy input and therefore considerable heat generation, can the proposed photobioreactor design allow for maintaining the culture temperature within reasonable bounds? Finally, to what extent can the concept be scaled, particularly regarding light intensity? To address these questions, Computational Fluid Dynamics (CFD) will be employed. Owing to its flexibility and maturity, CFD has already been widely and successfully used in the microalgae field, notably for optimizing or designing raceway ponds [42,43], bubble columns [44,45], static mixer-based photobioreactors [46,47], Taylor reactors [48], baffled airlift flat-panel photobioreactors [49], and torus-shaped photobioreactors [50], among others. The keen reader is referred to the review by Gao et al. for a broader overview of the topic [51]. Still, while the deployed methodology is not new, some rarely mentioned aspects of it, such as the existence of Lagrangian Coherent Structures [52] and their numerical implications will be explored.

2. Experimental proof-of-concept & Up-scaled design requirements

2.1. Experimental proof-of-concept

The experimental proof-of-concept was carried out *Chlorella vulgaris* 211-11b, bought from SAG Culture Collection, Germany. The cells were grown under 7000 μmolPhotonPAR/m^2/s. Continuous and flashing light patterns were applied (square pattern, duty cycle of 0.5, frequency from 0.01 Hz to 1 kHz). Three control configurations were tested, all under continuous light: 200 μmolPhotonPAR/m^2/s (conventional cultivation conditions), 4000 μmolPhotonPAR/m^2/s (about the same average amount of energy), and 7000 μmolPhotonPAR/m^2/s (maximum incident light intensity, cells did not grow). The experiments were conducted in ultra-thin flat-panel photobioreactors (6-mm light path), operated in turbidostat (maximum optical density of 0.1) to ensure iso-actinic growth conditions. After acclimation, numerous outcomes were monitored, of which growth rate and pigment content are of interest for this article. The results showed that *Chlorella vulgaris* can grow at a similar rate under 200 μmolPhotonPAR/m^2/s of continuous light and under 7000 μmolPhotonPAR/m^2/s of flashing light for frequencies between 0.1 and 100 Hz (growth rate of 2 1/day). In addition, super high light cultivation reduced the cell chlorophyll content (to 2.56 ± 0.29 mg/g for total chlorophyll under 1 Hz) while increasing the carotenoid ones. While all the other indicators are of interest, for the sake of brevity, the kind reader is referred to the original article to know more about them [27].

2.2. Up-scaled design - fluid flow & light/dark patterns

Before diving into the numerical fine-tuning of the prototype blueprint, it is important to evaluate which photobioreactor family is best suited for reproducing the conditions of the proof-of-concept at a larger scale. The selection criteria are: the possibility of easily creating high-frequency (0.1 Hz or more) light cycling patterns; the quality of these patterns (*i.e.*, low dispersion of cycle parameters such as frequency and duty cycle); gas transfer capability (to supply carbon dioxide to avoid carbon limitation while removing oxygen to prevent inhibition); and ease of thermal management.

With these criteria in mind, open raceway ponds can be ruled out, as they do not allow the generation of homogeneous, high-frequency light patterns [42]. In addition, unless sumps are integrated into the design, gas transfer can also be considered suboptimal [53,54]. Supplying carbon dioxide and removing molecular oxygen could likewise become problematic in horizontal tubular photobioreactors, which would

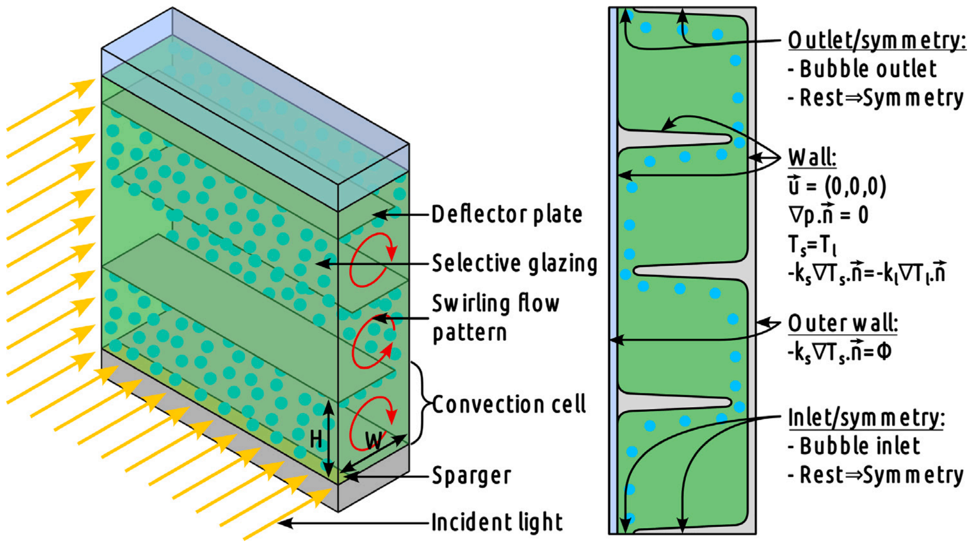

Fig. 1. Left - Baffled flat-panel design schematic, featuring three convection cells. H - Convection cell height. W - convection cell depth. Right - Cut view and model boundary conditions.

require frequent degassing units [25]. Furthermore, although static mixers can be used to induce swirling flows which, combined with the light gradient inside the reactor, generate light cycles, the progressive dissipation of azimuthal momentum would necessitate frequent mixing units [46,47]. This would result in high pressure losses and complex cleaning operations.

In this context, designs featuring bubble-driven agitation become particularly appealing because of their high gas transfer potential. Indeed, even a simple bubble column can induce light cycling patterns [45], even though not extremely stable. When precise control over the light pattern is required, baffled photobioreactors, particularly flat-panel designs, perform well [49,55] (Fig. 1 - Left). Among them, however, airlift variants (*i.e.*, featuring a clear separation between riser and downcomer sections) should be avoided due to the fact that one section places the culture in darkness would alter the light cycling pattern by introducing a prolonged dark phase [49]. Consequently, the baffled flat-panel photobioreactor emerges as a promising candidate among conventional designs.

This type of photobioreactor is built around a central element: the convection cell, a cavity featuring a gas inlet at the bottom on one side and a gas outlet at the top on the other side. This configuration allows bubbles to entrain the liquid into a swirling motion while remaining confined inside the cavity. By illuminating the vessel from one side, thereby creating a light gradient across the convection cell, and because microalgae closely follow the flow structure, individual cells experience a repeating light/dark cycle indefinitely.

Of course, the convection cell design must be chosen with care. First, the combination of its geometry (particularly the depth-to-height ratio) and the penetration depth of the light gradient determines the duty cycle of the resulting light pattern. The frequency of the pattern is more difficult to predict, as it emerges from a subtle interplay between convection cell perimeter, wall shear stress, and bubble-transferred momentum. Nevertheless, asymptotic cases can be envisioned. If the convection cell diameter is too small, wall friction dissipates liquid momentum and slows the swirling motion, resulting in low light-cycle frequencies. Conversely, if the convection cell is too large, bubbles can accelerate the flow only to a limited extent because gas-phase slip velocity is constrained by physical parameters (mainly air–water surface tension and gravitational acceleration). As a result, liquid velocity becomes capped, and light-cycle frequency again decreases with increasing convection cell size. Finally, from a thermal management perspective, larger convection cells are advantageous because they increase the thermal inertia of the system, thereby limiting sharp temperature fluctuations.

Once the physical trade-offs have been acknowledged, two last considerations are to be addressed: realizability and ease of cleaning. Both command a reactor to be large enough so that design and assembly come in handy, and cleaning in place can be performed efficiently (nullifying dead zones by forcing liquid high liquid flow rates, and scrubbing being possible as a last resort). Therefore, a square convection with a depth/height of 5 cm was chosen, with a width of 50 cm and a height of 50 cm (filled up to 40 cm to reach a 10-liter working volume, ideal for a lab-scale prototype). With the key dimension determined, the next step is to identify a cell concentration allowing for a duty cycle of 0.5, *i.e.*, ensuring that about half of the photobioreactor depth is illuminated.

Computing the light field within a reactor is not an easy task, as it requires solving the Radiation Transport Equation (a.k.a. RTE). Still, recently, a dimensionless correlation (Eq. (1)), summarizing 3240 simulations, was introduced to offer an easy-to-compute light field within this type of system [56]. It covers various cell concentrations, strains, pigment profiles, and void fractions (assuming spherical bubbles), and can be applied to virtually any visible wavelength, thanks to the work of scholars having tackled the wavelength dependency of the microalgae spectral properties [57–59].

$$\frac{I(z)}{I_0} = (1 - \underbrace{\phi(\frac{\sigma_S}{\sigma_A})}_{\text{Reflection by the cells}} - \underbrace{\zeta(\frac{\alpha}{\sigma_A C d})^{4/3}}_{\text{Reflection by the bubbles}}) exp[-\sigma_A C z \underbrace{(1-\alpha)}_{\text{Bubble effect on absorption}} (1 + \underbrace{\gamma\frac{\sigma_S}{\sigma_A}}_{\text{Cell ray path lengthening}} + \underbrace{\omega\alpha exp(-\sigma_A C d)}_{\text{Bubble ray path lengthening}})] \quad (1)$$

whence $\phi = 1.888\ 10^{-3}$, $\zeta = 2.365\ 10^{-2}$, $\gamma = 0.02046$, and $\omega = 5.830$.

Using this correlation requires only knowing the cells' absorption and scattering cross sections and the bubble diameter (see later). In this respect, the work of Baránková et al. is of peculiar importance [58]. Indeed, it is the only one providing spectral data as a function of the cell pigment content, which is key here, as the cells born of the proof-of-concept have a special pigment profile. Focusing on blue light, which the most absorbed by the chlorophylls (around 437 nm), the pigment specific absorption and scattering cross sections are 329.7 and 1243 $cm^2/(mg_{Total\ chlorophyll}/g)$, which, combined with the 2.56 ± 0.29 mg/g for total chlorophyll (under 1 Hz) of the cells leads to the absorption and scattering cross sections values.

The illumination being a continuous value distributed in a monotonically decreasing fashion within the system, the last step is to determine the value below which the environment can be considered dark for the cell. While complicated to precisely measure, the compensation intensity (when photosynthesis surpasses maintenance) can be evaluated around 5 to 10 μmolPhotonPAR/m^2/s for *Chlorella vulgaris* [55]. Still, while it would boost the results from this article, a safer threshold was retained owing to the cell's very low pigment content: the saturation intensity (around 100 μmolPhotonPAR/m^2/s for *Chlorella vulgaris* [55, 60]). With all these elements, it can be estimated that a microalgae concentration of 1.14 g/L would allow a somewhat exponentially attenuated light field of 7000 μmolPhotonPAR/m^2/s incident intensity to reach 100 μmolPhotonPAR/m^2/s at a depth of 2.50 cm. Consequently, half of the photobioreactor depth would be illuminated, leading to an expected duty cycle of 0.5, similar to the one in the experimental proof-of-concept.

2.3. Up-scaled design - thermal aspects

While hinted at in the previous section, the thermal aspects of the prototype are also to be carefully considered. Indeed, massive light delivery will come hand in hand with massive heat delivery. Fortunately, several techniques can mitigate this problem. First of all, cold mirrors (mirrors reflecting only the visible part of the spectrum, with a sharp cut at 750 nm) can be used to reflect only the part of the sunlight onto the prototype [61]. In addition, UV-repelling glass can be used for the photobioreactor conception to repel some more heat and incidentally addressing the question of high UV dosage-induced mutagenesis [62]. Together, these two measures allow for a reduction by 61.5% the solar heat load (under 1.5 atmospheric mass) by narrowing it down to the useful visible radiation only. Still, even when restricted to the visible part of the spectrum, actinic illumination will carry substantial heat that will have to be dissipated in order to maintain the cell in its ecological niche (above 15 and below 35 °C [63]). Limited options are available on the illuminated side of the photobioreactor, as light supply is kept as unaltered as possible. Therefore, natural convection and radiation are the only modes of transfer considered. On the contrary, the backside of the photobioreactor can allow for several heat dissipation techniques, such as natural convection, fin stack, forced air, or water cooling (Fig. 2 - detailed hereinafter).

3. System model

With the system set up, the next step was to formulate a numerical model capable of simulating its behavior. The first step is to choose among the different families of multiphase flow modeling frameworks (the phases being: liquid - culture medium -, gas - sparged air -, and solid - microalgae -). Among them, interface-resolving methods (*e.g.*, Volume of fluid [64]) can be ruled out as they would not allow for simulating a domain large enough. Euler-Euler methods do not describe bubble positions *per se* [65] but a phase indicator field instead, which would require specific numerical treatment to account for precise microalgae motion. Euler–Lagrange approaches are the only ones capable of simulating a large domain and precisely locating the bubbles and microalgae within it (with minimal assumptions), at the price of considering every Lagrangian particle as punctual. It was therefore retained for this work.

Once fluid flow model has been chosen, the next step is to model internal illumination. As detailed in Section 2.2, this work was carried out previously, and the resulting correlations will be used (Eq. (1) [56]). Together, fluid flow and internal illumination allow for the reconstruction of the light/dark cycle experienced by the cells and assess if the design is able to generate the patterns previously identified as adequate over the course of the experimental proof-of-concept.

Heat management comes next. First, the system is modeled in its entirety using a Conjugate Heat Transfer (a.k.a. CHT), where heat absorption in liquid, its convection by the flow, and conduction in the solid are considered altogether at once. Fourier's law was employed to describe conduction, as, even under the highest heat flux envisioned in this application, its validity is not challenged [66]. Overall, this approach will demonstrate that the system is quite homogeneous from a thermal standpoint (even in the worst-case scenario) and could therefore be modeled using a thermal circuit or a set of Ordinary Differential Equations (a.k.a. ODEs).

3.1. Continuous phase model

The Eulerian approach is used for the continuum (culture medium), while the dispersed phases are described as Lagrangian particles (sparged air and microalgae). Equations and numerical specificities have been published previously [67] and are presented in the Supplementary Materials; only the main features will be presented here. The liquid flow is modeled using classical incompressible Navier–Stokes equations (see Fig. 1 - Right, for boundary conditions, and Table 1 for physical properties). The growth medium was described as a Newtonian fluid. While valid for low-concentration cultures (below a volume fraction of 0.70% for freshwater *Chlorella* sp.) [68], this assumption could be discussed for high-density ones. Fortunately, such values are not encountered here as the targeted concentrations will remain below this threshold. Furthermore, bubbles contribute to the evolution of the continuous phase momentum in a two-way coupling (based on the reciprocal forces exerted by one another). Finally, turbulence was not encountered in the flow as the maximum bubble Reynolds number remained far below the critical Reynolds numbers values. In addition, no turbulence was originating from the bubble. While this statement may seem contradictory to the existence of Bubble Induced Turbulence (a.k.a. BIT) models, one has to remember that those models are intended to account for the complex bubble swarm wakes intertwining (referred to as pseudo-turbulence) in Euler-Euler simulations [69].

3.2. Dispersed phases model

Bubbles and microalgae are described using a Lagrangian approach. The particles are assumed to be spheres subjected to several forces: buoyancy, virtual mass, and drag. The main difference between the two phase being their density (1.2 kg/m^3 for the air, 1030 kg/m^3 for the air for the microalgae [70]), their diameter (1.383 mm for the air - see below -, 3.4 μm for the microalgae), and the drag force correlation (bubble correlation for the air, solid sphere correlation for the microalgae - see Supplementary Materials).

Assuming the bubble to be spheres places a constraint on their Bond number, it should be below 1, leading to a maximum diameter of 2.71 mm. This value is to be compared to that of classical bubbles generated by industrial spargers made of sintered steel (pore diameter from 1 to 60 μm, 15 to 45% porosity from manufacturer's datasheet). In order to be conservative, only the largest pores are considered to generate bubbles (*i.e.*, 60 μm), and the porosity is taken in the middle of the range (30%). By designing the sparger so that it spans over a tenth of the depth and across the whole width (Fig. 1 - Left) with an aeration set at 0.1 VVM (Vessel Volume per Minute, sufficient to limit dissolved oxygen around 123% of the saturation - see Supplementary Materials), it is possible to derive the air velocity at the orifice level. Assuming the fluid's properties are similar to those of water, the bubble diameter can be calculated using Shyu *et al.*'s work (Eq. (2)) [71]. The obtained value is 1.383 mm, which leads to a Bond number of 0.26. In addition to the value itself, its sensitivity is to be assessed, especially given the assumptions that were drawn. The most sensible part is the evaluation of the air velocity at the orifice level. Yet, to get a +5% deviation on the bubble diameter, one must increase the aeration from 0.1 to 84 VVM. Obtaining such a minor deviation for such an increase in the input flow rate shows the robustness of this estimation.

$$d = \sqrt[3]{\frac{(\pi + 1.31 Bo Fr) D^3}{Bo}} \quad (2)$$

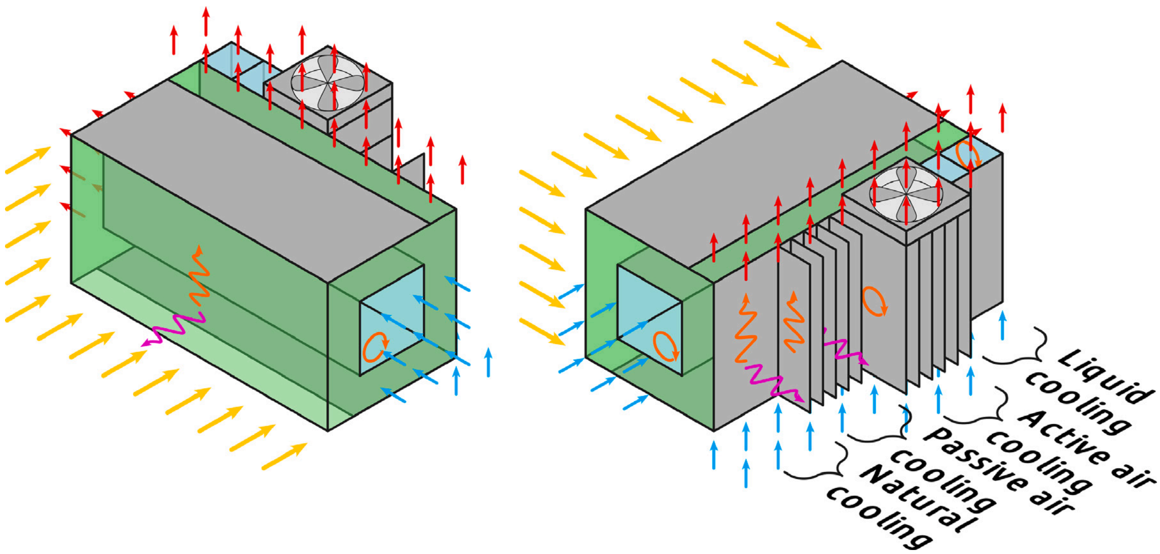

Fig. 2. Left - Front-side view of a convection cell. Right - Backside view of a convection cell. Blue arrows - Cold cooling fluid inflow. Red arrows - Hot cooling fluid outflow. Yellow arrows - Incident light. Orange arrows - Convection (natural or forced). Wavy arrows - Radiation (purple) or natural convection (orange). Circular arrows - Forced convection.

whence Fr is the Froude number, D is the orifice diameter (60 μm). One should note that, fortunately, this correlation was validated for orifice diameters down to 60 μm.

3.3. Heat transfer

Two approaches were used sequentially to tackle questions dealing with the thermal behavior of the system. First, the solid (glass and aluminum) and fluid (considered water) parts of the system were modeled together in a transient Conjugate Heat Transfer framework (equation available in Supplementary Materials). The illuminated side boundary condition was taken as the sum of natural convection (for vertical flat plates, Eqs. (3) and (4) [72]) and radiation (Rosseland approximation, Eq. (5)) with a surrounding environment featuring a constant temperature of 20 °C (Fig. 2 - Left). The backside could be fitted with several heat dissipation mechanisms (Fig. 2 - Right), among which natural convection, fin stacks (design procedure drawn from Bar-Cohen and Rohsenow's guidelines [73]), forced air or liquid cooling were considered. The backside heat exchanger was considered made of 1-cm side square tubes vertically welded together, because of the ease of realization and modeling of the system (using Gnielinski's correlation [74], Eq. (6), where the wall Prandtl number is assumed to be equal to the bulk one and the tube length is much longer than the tube diameter, f being derived from Eq. (7)). The cooling flow rates were chosen as 3.8 m^3/h for liquid, and 1800 m^3/h for air, as easily commercially available pumps/fans can achieve them. Second, as it has been hinted at previously, the Conjugate Heat Transfer simulations will demonstrate that the components of the system are homogeneous from a thermal point of view. Accordingly, its description can be simplified using a thermal circuit (resistance in series) methodology.

$$Nu = 0.68 + \frac{0.670\ Ra_x^{1/4}}{[1+(0.492\ Pr)^{9/16}]^{4/9}} \qquad Ra_x \leqslant 10^9 \tag{3}$$

$$Nu = \left[0.825 + \frac{0.387\ Ra_x^{1/6}}{[1+(0.492\ Pr)^{9/16}]^{8/27}}\right]^2 \qquad Ra_x > 10^9 \tag{4}$$

$$h = 4\sigma T^3 \tag{5}$$

$$Nu = \frac{(f/8)(Re-1000)Pr}{1+12.7\sqrt{f/8}(Pr^{2/3}-1)}\left[1+\left(\frac{D_h}{L}\right)^{2/3}\right]\left(\frac{Pr}{Pr_w}\right)^{0.11} \tag{6}$$

$$f = (1.82\ \log_{10}(Re) - 1.64)^{-2} \tag{7}$$

Table 1
Physical properties of the different materials at play. Properties values were determined close to 20 °C.

Phase	Property	Value	Unit
Culture medium (liquid)	Density	998	kg/m^3
	Dynamic viscosity	1.0 10^{-3}	Pa s
	Surface tension (with air)	7.2 10^{-2}	N/m
	Thermal conductivity	0.6	W/m/K
	Specific heat capacity	4183	J/kg/K
Bubble - air (gas)	Density	1.2	kg/m^3
	Dynamic viscosity	1.8 10^{-5}	Pa s
	Surface tension (with water)	7.2 10^{-2}	N/m
	Thermal conductivity	2.6 10^{-2}	W/m/K
	Specific heat capacity	1008	J/kg/K
	Diameter	1.383 10^{-3}	m
Aluminum (solid)	Density	2719	kg/m^3
	Thermal conductivity	202.4	W/m/K
	Specific heat capacity	871	J/kg/K
Glass – amorphous fused silica (solid)	Density	680	kg/m^3
	Thermal conductivity	1.4	W/m/K
	Specific heat capacity	2196	J/kg/K
Microalgae (solid)	Diameter	3.4 10^{-6}	m
	Density	1030	kg/m^3

3.4. Numerical implementation & convergence study

The CFD model was implemented into a custom solver built with OpenFOAM v2506 [75] with the geometry being simplified into a 2D case. The code uses a PISO strategy (Pressure-Implicit with Splitting of Operators) to solve momentum and mass continuity equations. Discretization was led using second-order schemes. As this implementation of OpenFOAM relies on an implicit segregated approach to solve the system of equations, scaled residuals of 10^{-6} or below, for all fields, were considered sufficient to ensure convergence of a given temporal iteration.

Initially, the system is still, and the bubbles are introduced in the system at the bottom inlet to satisfy the 0.1 VVM aeration rate. The simulation is run until flow descriptors enter a quasi-steady state (around 60 s - see Supplementary Materials) and is prolonged afterward by batches of 5 to 7 s (two characteristic timescales, due to the existence of Lagrangian Coherent Structures [52,76] - see Supplementary Materials). Mesh (automated procedure led with *snappyHexMesh* utility and six buffer cell layers [77]), Courant number, and domain size convergences are also detailed in the Supplementary Materials. Overall, the retained mesh features an extrapolated error of 1.04% [78] and a Grid Convergence Index (a.k.a. GCI [79]) of 1.31% on the most reluctant flow descriptor (liquid volume-averaged norm of vorticity), in the worst case scenario, which was deemed acceptable. Finally, it is important to note that CFD results were post-processed in line using OpenFOAM dedicated tools to ensure discretization schemes consistency, while domain visualizations were rendered using Paraview.

Once the fluid flow had been simulated and microalgae trajectories acquired, the light histories were reconstructed externally using Eq. (1). Afterward, 15 000 light/dark cycles were collected (the dark phase being defined as an illumination below 100 μmolPhotonPAR/m^2/s). This number allowed for a converged representation of the experienced patterns (see Supplementary Materials). In addition, as underlined recently by Shirian et al. [80], several non-overlapping extractions have to be performed in order to ensure the representativity of the observed pseudo-steady state. In the present case, 20 extractions were carried out and are reported using distribution descriptors (median and inter-quartile distance, as the frequency distribution is not Gaussian).

3.5. Partial validation

Implementing a workflow and ensuring its numerical convergence is only the first step towards creating confidence in the results it will generate. The second is to validate its predictions against canonical cases. This task is quite challenging in the case at hand because the process outcomes are light/dark cycles and thermal behavior. Yet, while no benchmark allowing for the validation of the workflow as a whole exists, partial validation can be carried out. This procedure relies on validating specific components of the model individually (Conjugate Heat Transfer and the fluid flow components, here). The choice of the benchmark to compare to is also delicate because it has to be both challenging (today, any code can reproduce a Poiseuille flow) and relevant (similar geometry, flow regime, way to set the flow in motion).

The Conjugate Heat Transfer part of the workflow was validated against the canonical case introduced by Susec in 1973 [81]. In this work, the author considered a 2D laminar slug flow of a hot fluid sweeping the upper face of a thin layer of highly conductive solid material while its lower face is cooled down convectively (Fig. 3 - Top left). Assuming an inviscid fluid, a low Biot number of the solid body, a high Péclet number, and constant physical properties, Susec has been able to derive an analytical solution for the fluid temperature over time, anywhere in the fluid domain. Taken together, these elements yield a very robust benchmark for the backside of the proposed design, which features almost like-for-like similarity: heat transfer through a solid cooled by convection on one side and a resolved laminar fluid flow on the other. While details are available in the Supplementary Materials (analytical solution, symbol meaning, and numerical convergence), Fig. 3 - Bottom left - presents the comparison between the workflow predictions and the analytical solution assuming the fluid to be water (flowing at 0.01 m/s), the solid to be aluminum, and intense convective cooling (1000 W/m^2/K), in a 10×100 mm^2 domain with a 1 mm thick solid. As one can see, for the selected probe positions, the workflow adequately predicts the dynamic and the final value of the water temperature. The only discrepancy is the smoothing of the stepwise temperature increase (corresponding to when the hot air reaches the probe location). Yet, it echoes the challenge that represents conserving a shock with a numerical scheme, which is fortunately not encountered in the intended application of the workflow.

Identifying a benchmark for the fluid flow was not as easy as for the Conjugate Heat Transfer part of the workflow. Indeed, few authors have investigated airlift reactors with detailed analysis tools, such as Particle Image Velocimetry (a.k.a. PIV) or Laser Doppler Anemometry (a.k.a. LDA). Among them, the possibilities are further restricted by the fact that bubbles are assumed to be spherical and that gas is the only means to entrain the liquid (some authors used gas and a magnetic stirrer [82]). Finally, among the references identified [83,84], only the work of Liew et al. provided sufficient details to ensure a reasonably faithful reproduction of the experimental device (Fig. 3 - Top right). The setup is relatively simple with a sparger on one side of the reactor and a fixed baffle to separate the riser from the downcomer. Only one level of water filling (46 cm) and one gas flow rate (0.30 m^3/h, assumed N m^3/h) were tested, while the outcomes were the velocity profile (using Laser Doppler Anemometry) on the symmetry plane of the reactor at three different heights. Finally, it is worth mentioning that the authors took care to add some salt to prevent bubble coalescence, but did not specify the average bubble diameter, though.

Fig. 3 - Bottom right - presents both experimental and numerical results. As one can see, the agreement is reasonable. The downcomer velocity profiles are overall well predicted, with trends well captured, but absolute value deviations for the two lowest profiles. The riser velocity profiles show a good qualitative agreement, but absolute values are off target most of the time. While not ruling out possible misdescription of the physical phenomena at play, the quality of the experimental data is to be considered. Indeed, some information is missing (*e.g.*, bubble diameter, sparger porosity, and pore size), and the reliability of measurements can also be challenged to some extent. Regarding the bubble diameter, a sensitivity analysis was carried out (1, 3, and 5 mm diameter, see Supplementary Materials), and 3 mm was selected based on the data reproduction quality. Regarding the measurements performed by the authors, they hint that the averaging window they chose (60 s) might have been too short. Indeed, as the bubble plume oscillates, a longer averaging time might have been needed to obtain a sufficiently converged value of the local velocity. This argument is supported by the sharp drop in velocity (−0.15 m/s) for 2 points around $x = 0.27$ m, for the z = 0.30 m line, or the surge in velocity (+0.10 m/s) for one data point (x = 0.28 m) for the z = 0.20 m line. Indeed, the plume might have shifted away from the laser spot when they carried out the measurements at these locations. This argument is further supported by the tracking of the numerical plume that suggests that a 60-second averaging might indeed be too short (see Supplementary Materials). To deliver converged results, the numerical profiles presented here were averaged for 200 s. Despite the aforementioned discrepancies, all in all, this partial validation allows to consider that the workflow delivers adequate results for the task at hand.

4. Preliminary results

4.1. System behavior

Once the accuracy of the numerical workflow has been ascertained, the next step is to apply it to evaluate the capabilities of the tentative design. The simulations were carried out by letting hydrodynamic enter a pseudo-steady state (60 s) before turning on the illumination (set at 3.5 times maximum sunlight, *i.e.*, 7000 μmolPhotonPAR/m^2/s effectively supplied to the culture) and activating active liquid cooling on the backside to maximize the thermal contrast. As numerous dimensions can characterize the intended system performance, they will be analyzed sequentially.

First of all, a qualitative visualization of the same system is proposed in Fig. 4 - Top. As one can see, the system behaves as expected with bubbles inducing the appearance of vortices at the center of the convection cells and driving microalgae into a circular motion. Carrying on with qualitative results, Fig. 4 - Bottom - presents the flow velocity vector field (square root scaling of legibility reason) and temperature profile (5 min after illumination onset, when the spatial contrast is the most pronounced - 0.25 °C spatial standard deviation -). This combined visualization confirms the existence of the macrostructures identified on the top panel of the Figure, but adds nuance to it. Indeed, small counterrotating vortices can be found in the corners of the convection

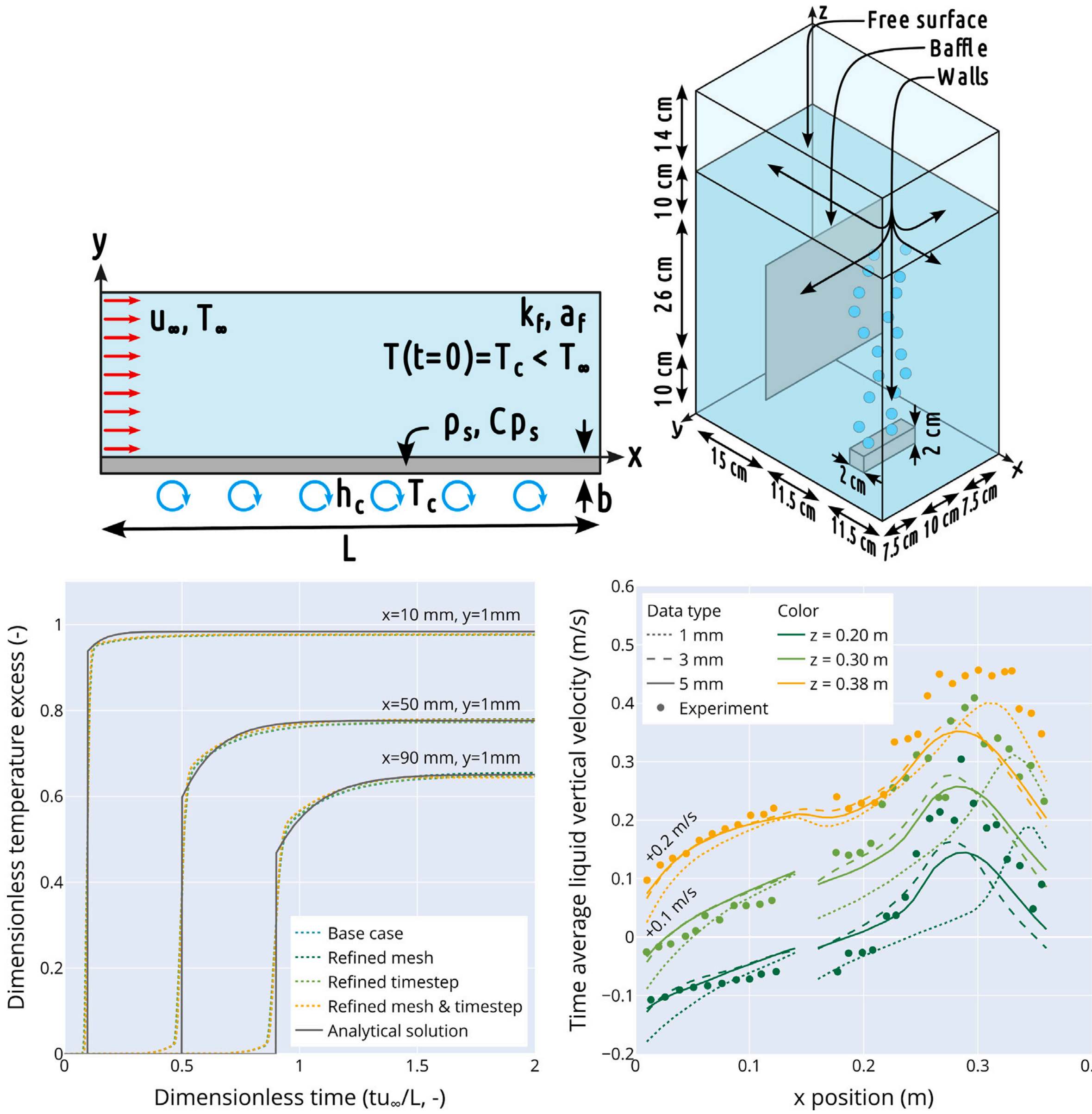

Fig. 3. Top left - Schematic of the setup for Conjugate Heat Transfer validation. Top right - Schematic of the setup for fluid flow validation. Bottom left - Results of the validation for the Conjugate Heat Transfer benchmark. Bottom right - Results of the validation for the fluid flow benchmark.

cells. Moving the temperature profile analysis, the cores of the vortices exhibit a lower temperature than the rest of the domain, even though the span remains moderate (1.2 °C). On the opposite side of the temperature range, some hot spots can be found in the vicinity of the glass (left side) and close to the location of the counterrotating vortices. While all these phenomena are self-explanatory and do not require much discussion, the fact that the numerical workflow identifies them is a token of its quality and opens the way to design fine-tuning.

With the flow and thermal components of the system behavior analyzed, it is time to focus on the light patterns induced by the system. First of all, because of the existence of Lagrangian Coherent Structures, the light cycles could only be extracted by batches (20 in total) of a two-characteristic-time duration each (*i.e.*, 5 s). Fig. 5 - Top - presents nine light histories (randomly drawn), with the shaded area corresponding to the dark phases of the cycles (taken as below 100 μmolPhotonPAR/m^2/s). With the binarization carried out, the light cycle frequency and duty cycle could be computed. Per batch, 15 000 cycles were agglomerated to construct a converged distribution of frequency and duty cycle among the population. One of the 20 distributions obtained with this protocol is presented in Fig. 5 - Middle & Bottom. As one can see, the frequency distribution exhibits a non-Gaussian trend with a median close to 0.51 Hz and a long tail nearing 1.5 Hz. As all the distributions are similar and exhibit a clear non-Gaussian profile, they were characterized using their median and interquartile distance. These two indicators are displayed in the figure's inset. As one can see, the distributions obtained from the 20 batches show narrowly distributed properties, confirming that they resemble one another. Moving to the duty cycle, the obtained distribution is somewhat Gaussian, centered close to 0.47, but spreading from 0 to 1. Here again, the medians and interquartile distances obtained on the 20 batches indicate that this behavior is shared among all the extracted batches.

4.2. Discussion

Before diving into considerations regarding the light/dark cycles, a comment is to be made on the system's thermal behavior. Indeed, a computationally intensive workflow has been deployed to entangle

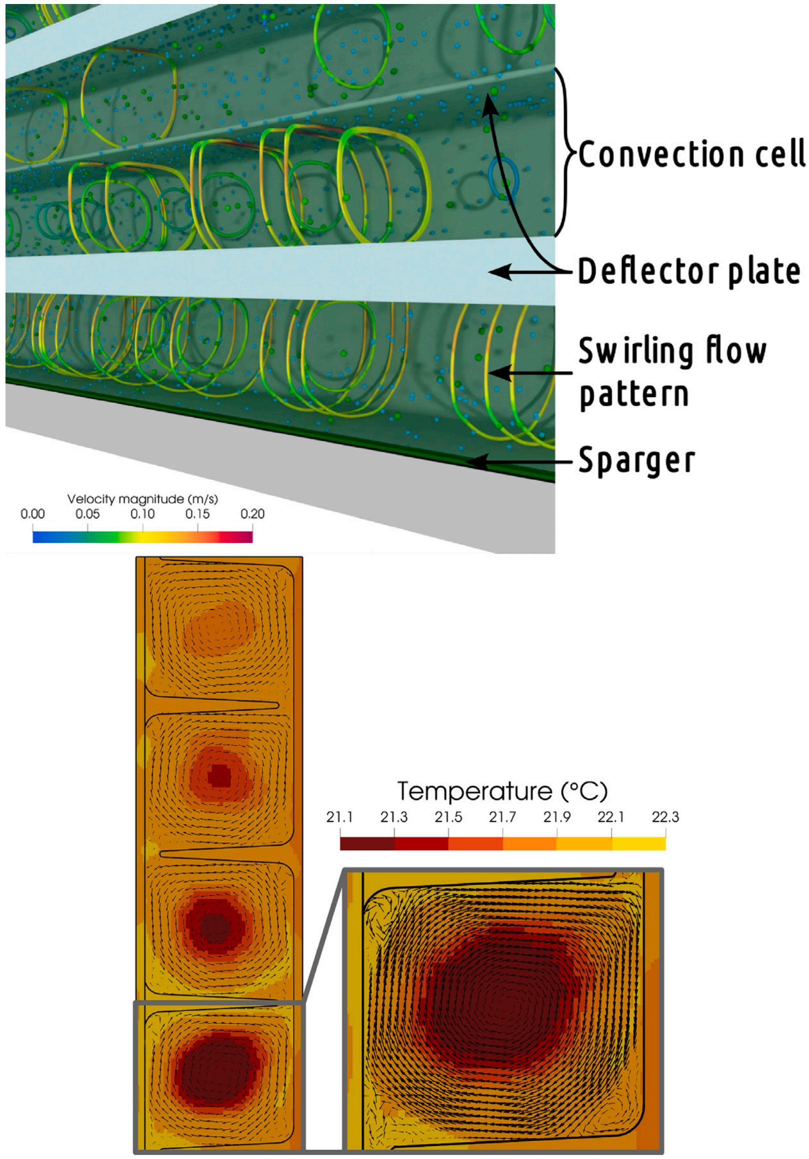

Fig. 4. Top - Illustration of the system behavior. Blue dots - bubbles. Green dots - microalgae (not scaled). Traces - Integration of the microalgae trajectories (randomly drawn), color by the velocity of the cells. Bottom - heatmap representing the temperature field 5 min after illumination induction (7000 μmolPhotonPAR/m^2/s) and vector map representing the velocity liquid field (square root scaling of legibility reason).

fluid flow, localized energy absorption, and combined conduction/convection. Yet, analyzing the resulting temperature distribution suggests that main components of the system (culture medium and backside aluminum frame) would be relatively homogeneous from a thermal standpoint (Indeed, the kind reader may note that the color range chosen on Fig. 4 maximizes an otherwise minor 1.2 °C temperature span). This observation opens the way to a much simpler modeling approach, such as a thermal circuit, potentially coupled with a system-wide energy balance. To test the relevance of such a simplification, a configuration exacerbating the temperature gradient was simulated.

On the one hand, a 40 000 μmolPhotonPAR/m^2/s illumination was cast onto the photobioreactor. While far outside the domain of validity of the biological proof-of-concept, this lighting configuration was intended as a stress test, maximizing the heat absorbed by the system. On the other hand, liquid cooling was considered implemented on the backside of the photobioreactor (resulting in a convective heat transfer coefficient of 979 W/m^2/K). So the starkest possible contrast between energy delivery and removal was ensured. Fig. 6 presents the thermal behavior of the system over time (using spatially average temperature and associated standard deviation as an indicator). As one can see, the average temperature rises steadily following the somewhat first-order response to reach 73.7 °C after about 1 h. In parallel, the temperature heterogeneity (spatial standard deviation, taken on a uniform grid) peaks at almost 1.5 °C after 5 min, before decreasing and stabilizing around 1.1 °C. All in all, it can be concluded that, even in the most contrasted cases, the system can be deemed homogeneous from a thermal standpoint.

Moving to the consideration of the light/dark cycles, the preliminary design allowed for important conclusions to be reached. On the positive side, the system indeed allows for the creation of light/dark cycles. On the negative side, the distribution of duty cycles is too wide to allow for fine control of the pattern (Fig. 5). The need to finely control the light/dark cycles is all the more important as super high light intrinsically bears a high risk of inducing photodamage if not delivered adequately. Indeed, while the experimental proof-of-concept showed that frequencies from 0.1 to 100 Hz could be used to safely drive the culture, only duty narrowly distributed duty cycles, in the vicinity of 0.5, can be considered safe at the moment. Therefore, instead of fine-tuning the design with the hope of marginal gains in terms of duty cycle control, a new one shall be proposed. While the results

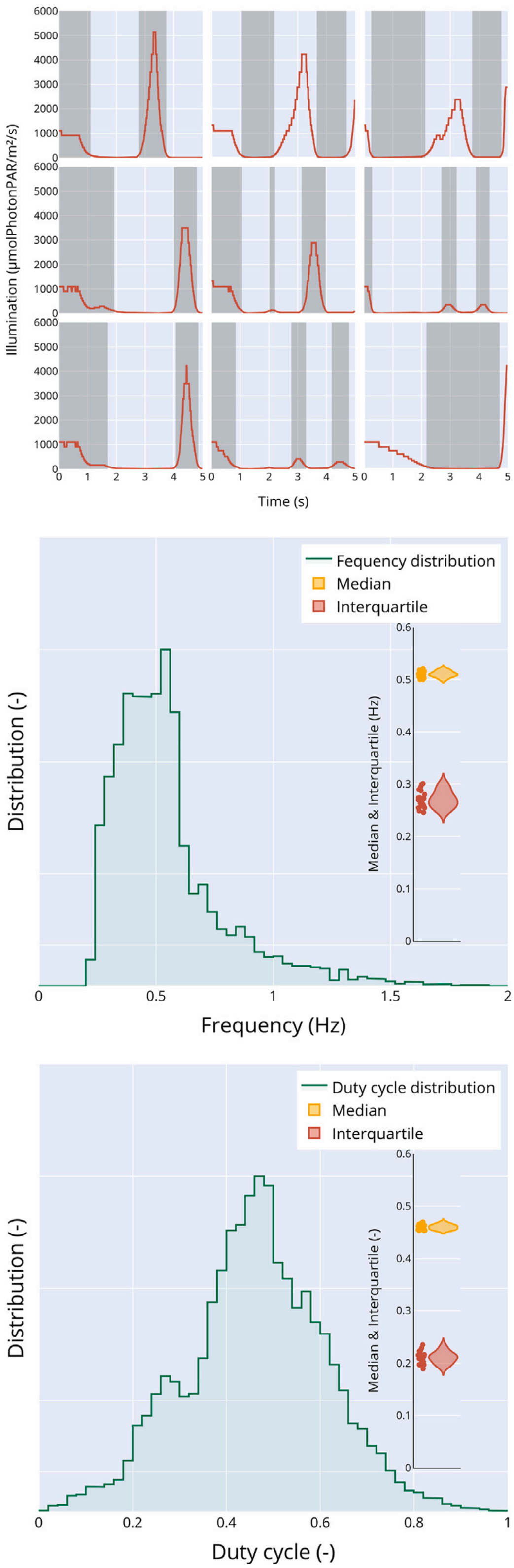

Fig. 5. Top - Nine randomly drawn light histories experienced by numerical microalgae. Shaded area - dark phase of the cycle (below 100 µmolPhotonPAR/m^2/s). Middle - One of the frequency distribution, built from 15 000 light cycles. Inset - Median and interquartile distance of all the distributions. Bottom - One of the duty cycle distribution, built from 15 000 light cycles. Inset - Median and interquartile distance of all the distributions.

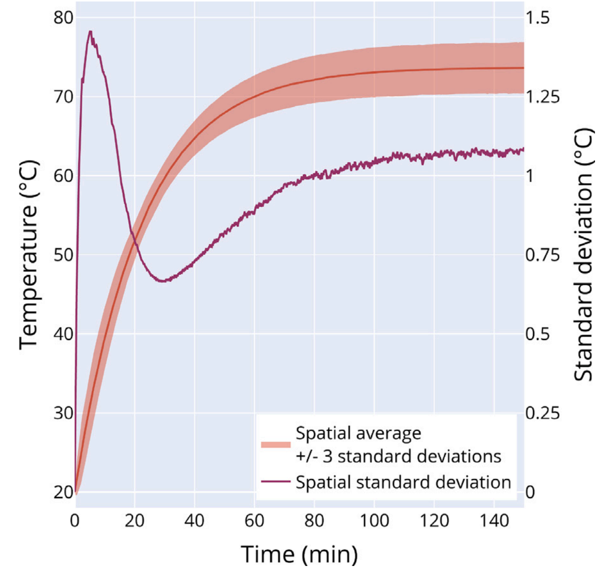

Fig. 6. Spatially average temperature and associated standard deviation for the extreme light delivery configuration (40 000 µmolPhotonPAR/m^2/s). At time 0, the system has already entered the hydrodynamic pseudo-steady state.

could be further discussed and the system behavior challenged (*e.g.*, modulating aeration to alter light cycle frequency or the geometry/cell concentration to alter the duty cycle distribution), the main points have been established.

5. Advanced design

5.1. Concept

Acknowledging the ability of the baffled flat panel photobioreactor to create light/dark cycles, the focus has been set on cross-fertilizing it with a design allowing for reducing the light patterns' duty cycle dispersion. In this regard, torus (a.k.a. annular or toroidal) photobioreactors have been reported as promising candidates [50,85]. These photobioreactors also revolve around the concept of a convection cell, but add a deflector tube at their core (Fig. 7). This way, from a hydrodynamic standpoint, the deflector tubes allow funneling the vortices at the centers of the convection cells into flow channels. These channels can be set in motion using an impeller [86], or, as in this case, a bubble swarm.

In addition to guiding the flow, the central deflector tubes can also be taken advantage of by circulating a cooling fluid (air or water) inside them, reinforcing the cooling possibilities. Also, the presence of the deflector tube *de facto* reduces the light path inside the culture medium. In this study, 3-centimeter square tubes are considered as deflectors, leaving 1 centimeter for the light path. This contraction of the light allows for an increase in the operating cell concentration so that all the light is absorbed (defined as falling below 100 µmolPhotonPAR/m^2/s) by reaching the tube. Adjusting the cell concentration with this procedure yields an operating concentration of 2.85 g/L.

Finally, while placing an inner deflector tube yields many benefits, it also induces one drawback. The additional surface area of the inner tube will contribute to dissipating momentum further and reduce the rotating liquid angular velocity for a given aeration. While negative from a system operation point of view, it is beneficial from a numerical modeling point of view, as, even with doubled aeration (0.2 VVM), the fluid velocities remain below the ones achieved in the preliminary design, ensuring the translatability of the meshing procedure.

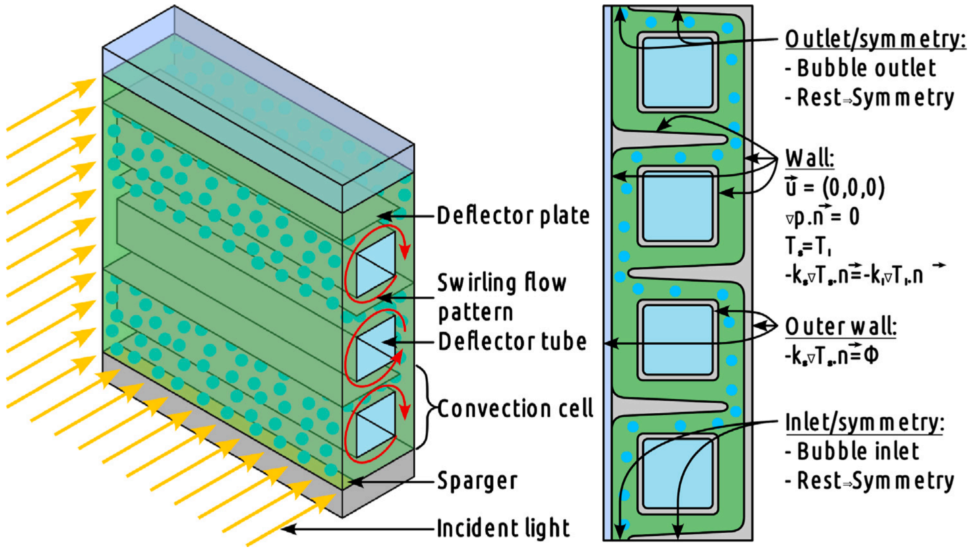

Fig. 7. Left - Advanced design schematic, featuring three convection cells. Right - Cut view and model boundary conditions.

5.2. System behavior

Fig. 8 presents the qualitative views of the system. As one can see, microalgae are cycled around the deflector tubes, with small counterrotating vortices persisting on the top of the convection cells. The temperature distribution is also modified compared to the preliminary design. While, the liquid temperature shows a lower thermal contrast, similar observations can be drawn overall. Hot spots are positioned next to the illuminated glass, close to the hydrodynamic recirculations. Yet, for the same duration of illumination (5 min in both cases), the new design achieves a lower overall temperature with a lower spatial contrast (22.43 ± 0.11 °C vs. 21.89 ± 0.25 °C). This can be explained by the fact that the inner parts of the convection cells have been replaced. Hence, large portions of fluid rotating onto themselves and only heated through conduction have been removed, explaining the improved homogeneity. Furthermore, the higher average temperature can be explained by the fact that, despite the additional heat transfer area offered by the deflector tubes, the total thermal inertia of the system has been reduced (5.9 liters of water versus 9.2 previously). Finally, the reduced thermal inertia shortens the system's thermal response time from 22 min 14 s to 8 min 30 s (assuming first-order dynamics), while remaining fully compatible with conventional closed-loop temperature control strategies.

Moving to the induced light/dark cycles (Fig. 9), one can see that the design modulation allowed for the imposition of much more narrowly distributed patterns, especially regarding the duty cycle. Also, the median value of the duty cycle has been modified (0.28 vs. 0.47 for the preliminary design), while the median cycle frequency is similar (0.47 Hz vs. 0.51 Hz for the preliminary design). Indeed, increasing the cell density within the photobioreactor shortened the depth of the illuminated zone, hence the average duty cycle. Nevertheless, it can be concluded that the proposed design allows for a much tighter control over the light/dark cycles characteristics.

5.3. Light/dark cycle modulation

With a now established design concept, the ability to modulate the light patterns by acting on its characteristic parameters is to be assessed. Intuitively, two levers can be acted upon: the injected gas flow rate - to modulate the cycle frequency -, and the deflector tube height-to-width ratio - to modulate the duty cycle -. As a first exploratory step, the two variables were varied independently (Table 2), from 0.05 to 0.2 VVM for aeration, and from 1/2 to 3/2 for the height-to-width ratio (keeping an inner tube height of 3 cm and a light path of 1 cm, Fig. 10). Results are presented as the average of the medians of the distributions obtained for each of the 20 data extractions ± the average of the associated interquartile distances. Also, within brackets, a pseudo-coefficient of variation is proposed (defined as the average interquartile distance divided by the corresponding average median) to get a sense of the relative spread these two quantities amount to.

Focusing on the effect of aeration, it effectively modulated the median cycle frequency, with a somewhat linear pattern (slope of 1.95 Hz/VVM). This trend can be explained by the fact that the flow is in a laminar regime. Therefore, transferring more momentum from the gas to the liquid leads to an increase in velocity and the associated gradients, but does not modify the flow pattern, hence scaling linearly. Of course, this behavior will reach lower and upper limits, and not all frequencies can be made accessible by modulating the aeration. The lower limit would be reached when bubbles would be too few to form a swarm that would entrain the liquid in its wake. The upper limit would be reached when bubbles are too numerous and merge to create gas pockets, whose ability to entrain liquid is diminished compared to a bubble swarm. Moving to the duty cycle, it is worth noticing that modulating aeration does not alter its mean value, nor its interquartile distance significantly.

Focusing on the effect of geometry modulation, it effectively acts upon the light/dark cycles parameters (ranging from 0.200 to 0.430 over the tested designs). As expected, reducing or expanding the length of a convection cell while maintaining its illuminated fraction constant (1 cm facing the glass panel) *de facto* leads to a modification of the duty cycle. Still, one can note that the median cycle frequency is also influenced by this lever. Indeed, for a fixed liquid velocity, lengthening or shortening the recirculation channel also modifies the cycle frequency (despite absolute aeration - m^3/h - adjustment, but keeping the relative one - in VVM - constant). This can be explained by the fact that altering the geometry may exacerbate or attenuate secondary flow structures, themselves changing the momentum dissipation patterns, hence the average liquid velocity. Therefore, it can be concluded that geometrical adjustments are a valid means of acting upon the light/dark patterns duty cycle. However, caution should be taken not to disturb the flow. Together with the observation of the counterrotation vortices inducing hot spots, this last comment underlines the relevance of CFD as a design tool to tackle the challenge of super-high-light photobioreactor conception.

Finally, the spread of the distributions is to be commented on. By closely examining Table 2, one can note that the interquartile distances are influenced in the same manner as the median values they

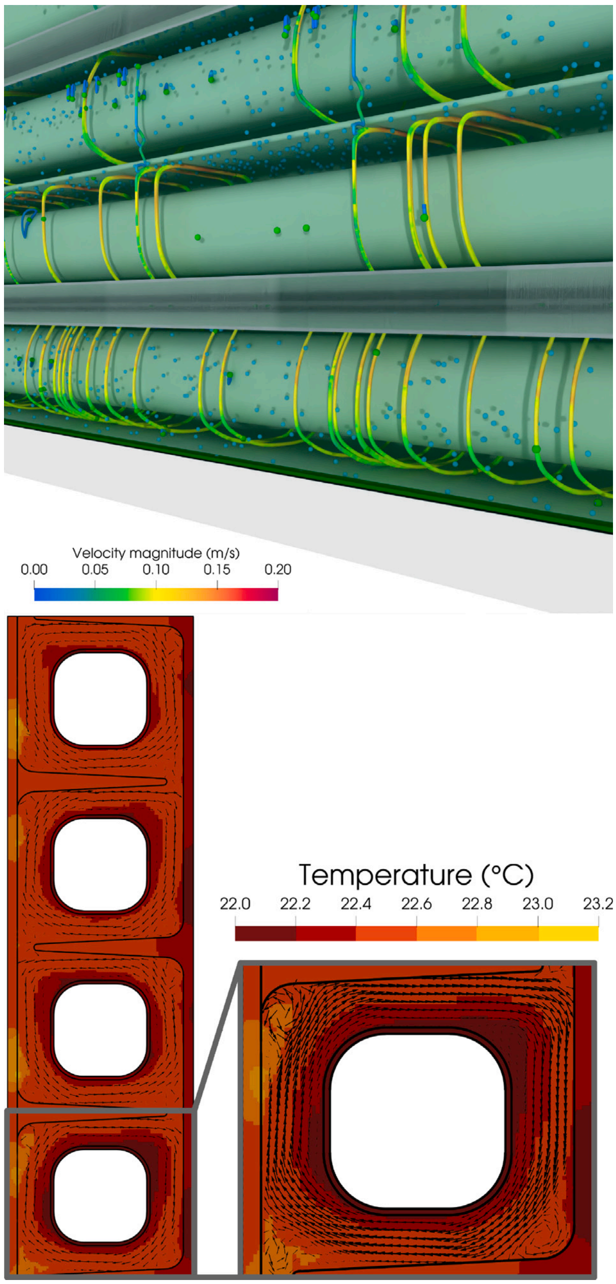

Fig. 8. Top - Illustration of the system behavior with the deflector tubes. Blue dots - Bubbles. Green dots - Microalgae (not scaled). Traces - Integration of the microalgae trajectories (randomly drawn), color by the velocity of the cells. Bottom - Heatmap representing the temperature field 5 min after illumination induction (7000 μmolPhotonPAR/m^2/s) and vector map representing the velocity liquid field (square root scaling of legibility reason).

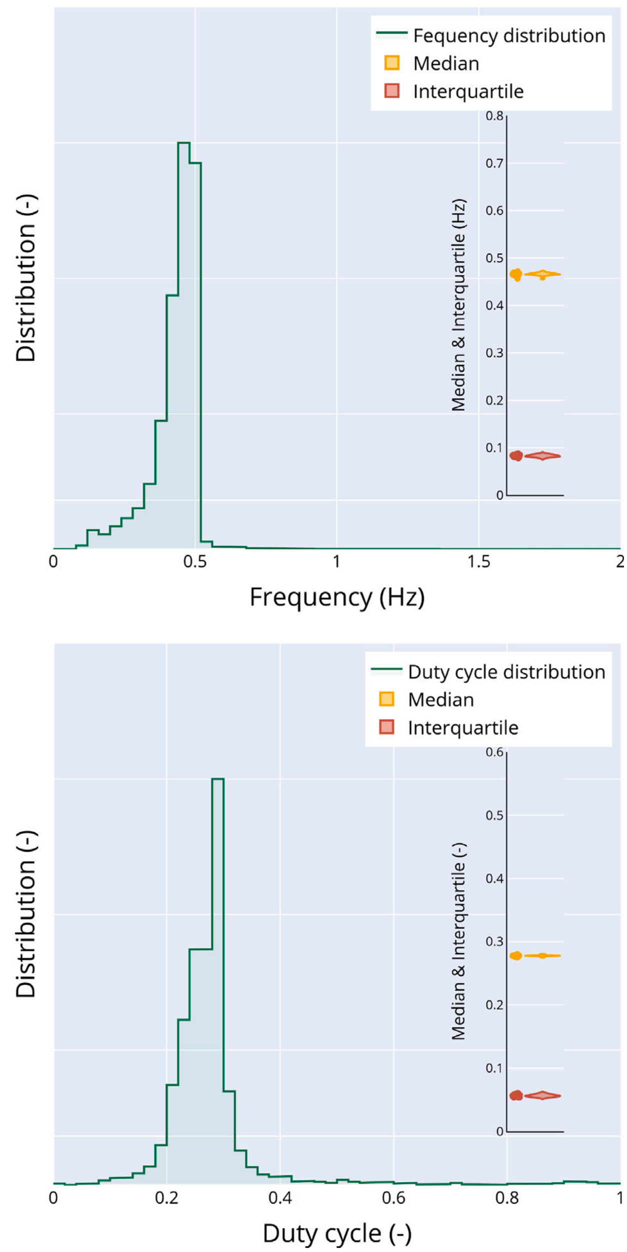

Fig. 9. Top - One of the frequency distribution obtained with the design featuring deflector tube (0.1 VVM), built from 15 000 light cycles. Inset - Median and interquartile distance of all the distributions. Bottom - One of the duty cycle distribution, built from 15 000 light cycles. Inset - Median and interquartile distance of all the distributions.

are associated with. To get a better sense of proportion, the pseudo-coefficient of variation is to be examined. Overall, acting upon aeration does not alter the spread around the median values significantly (from 17.4% to 22.8%, depending on the indicator and the aeration), while acting upon the geometry induced higher dispersion (from 17.7% to 32.4%, depending on the indicator and the aeration). Still, in any case the spread remain relatively high by biotechnology standard (aiming at a 10% dispersion). Yet, fortunately, it does not endanger the photobioreactor operation as, for example, the lowest frequency (0.322 Hz)

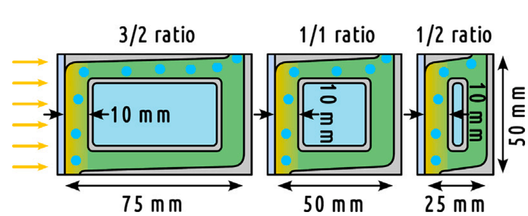

Fig. 10. Schematic view of the convection cell designs for the three tested height-to-width ratios.

Table 2
Design parameters and operating conditions varied to modulate light patterns. Results presented as average median ± average interquartile distance, over 20 extractions. Within brackets, a pseudo-coefficient of variation is proposed, defined as the average interquartile distance divided by the corresponding average median.

Goal	Convection cell width (mm)	Aeration (VVM)	Frequency (Hz)	Duty cycle (–)
Modulating frequency	50	0.2	0.625 ± 0.131 (21.0%)	0.271 ± 0.061 (22.8%)
		0.1	0.466 ± 0.082 (17.7%)	0.278 ± 0.056 (20.3%)
		0.05	0.322 ± 0.065 (20.3%)	0.279 ± 0.048 (17.4%)
Modulating duty cycle	25	0.1	0.404 ± 0.127 (31.5%)	0.430 ± 0.110 (25.7%)
	50		0.466 ± 0.082 (17.7%)	0.278 ± 0.056 (20.3%)
	75		0.409 ± 0.118 (29.0%)	0.200 ± 0.065 (32.4%)

to which the interquartile distance (0.065 Hz) would be subtracted, remains above the minimal frequency identified over the course of the proof-of-concept (0.1 Hz).

5.4. Maximum light operation

With the light patterns shown tunable, the remaining question is the upper value of incident light intensity the system could bear. Two strategies can be deployed to tackle this question. Either devising an incident illumination and determining the equilibrium temperature, to be hopefully low enough to allow the cell to grow. Or, setting the maximum operational temperature and identifying the corresponding incident illumination. While the two methods are essentially equivalent, the second option was chosen as it is easier to implement.

Thus, a thermal circuit model of the system was written. The core component is the culture medium, which can exchange heat on its two sides and with the deflector tube. On the illuminated side, the thermal resistances are located between the culture medium and the glass sheet, within the glass sheet (3 mm), and with the surrounding (natural convection and radiation). On the backside, the thermal resistances are located between the culture medium and the aluminum frame, within the aluminum frame (3 mm), and with the heat exchanger. Finally, the resistances mediating heat transfer between the culture medium and the deflector are located between the culture medium and the tube (aluminum), within the tube thickness (2 mm), and within deflector tube. The thermal resistance originating from convection within the culture medium is described assuming a fully developed laminar flow in an infinite channel (Nu = 7.54) [72].

Several scenarios were drawn with a culture medium temperature of 30 °C and a surrounding temperature of 20 °C. First, multiple designs of the backside heat exchanger were explored: bare plate, fin stacks, forced air, or liquid cooling within 1-cm square tubes (as illustrated in Fig. 2. Then, air or water was considered as a cooling fluid circulating within the heat exchanger and the deflector tubes. Also, the possibility of using a corrugated tube (+36% heat transfer efficiency) for the deflector tube and the backside heat exchanger was considered [87] (referred to as *boosted*). Finally, as a safeguard procedure, the preliminary design was also tested to validate the process (as a reminder 7000 in μmolPhotonPAR/m^2/s let the culture medium temperature reach 29.4 °C).

Fig. 11 presents the incident illumination allowing a 30 °C temperature for the culture medium in the advanced design photobioreactor for the different cooling strategies and for the preliminary design. First of all, the case of the preliminary is to be examined as it can inform on how close the Conjugate Heat Transfer simulation and the thermal circuit model are. For this configuration, the thermal circuit model predicts a maximum illumination of about 9000 μmolPhotonPAR/m^2/s while the Conjugate Heat Transfer simulation allowed to determine a value of 7000 μmolPhotonPAR/m^2/s. While not in perfect agreement, the two values can be deemed close, especially given the difference in complexity between the two approaches. Furthermore, the discrepancy can be explained by the fact that the thermal circuit model assumes a fully developed laminar flow within the culture medium, while the

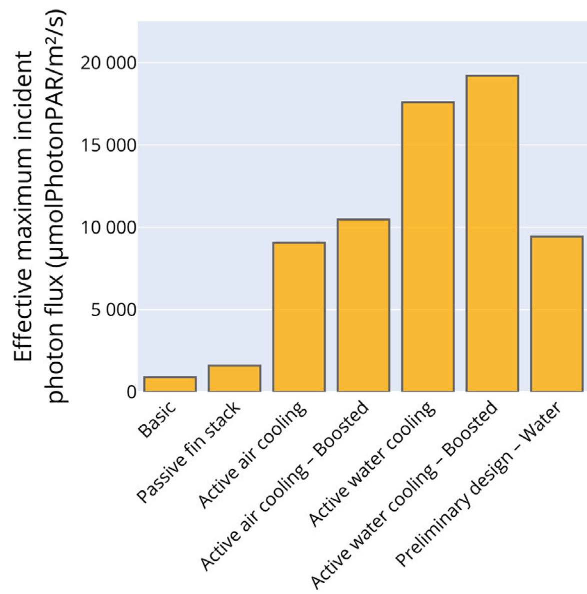

Fig. 11. Maximum incident illumination allowing to reach a 30 °C temperature for the culture medium in the advanced design photobioreactor.

Conjugate Heat Transfer simulation is able to describe counterrotating vortices, hindering heat transfer. In a sense, the thermal circuit model predictions can be considered as a good approximation of the system performances if the hydrodynamic circulation were improved.

Moving to the comparison between the cooling strategies, they allow reaching from 900 to 19 200 μmolPhotonPAR/m^2/s as the maximum illumination achievable, while keeping the culture medium temperature at 30 °C. Among them, purely passive techniques (bare backside and fin stacks) are located at the lower end of the range (900 and 1600 μmolPhotonPAR/m^2/s, respectively), while active air cooling holds the middle ground (9000 and 10 500 μmolPhotonPAR/m^2/s), and are surpassed by the liquid cooling options (17 500 and 19 200 μmolPhotonPAR/m^2/s). This segregated pattern is not uncommon and can be encountered in other domains facing challenges, *e.g.*, computer silicon cooling, which resorted to water cooling owing to its higher thermal conductivity.

Finally, the gain offered by the use of internally corrugated tubes is to be discussed. Considered on their own, they deliver an improved heat transfer coefficient (by +36%). Still, as they are included in a system, the end result is to be considered. When employed in the backside heat exchanger, they deliver limited gain (+12% for air and +6% for water), underlining that it is thermal resistance between the culture medium and the aluminum frame that controls the heat flux. When this enhancement is used in the deflector tubes, the gains are larger, but still modulated by the fluid nature (+30% for air and +14% for water). Overall, the relevance of this type of options is definitely case dependent in the context of a super-high-light photobioreactor, but they virtually allow to achieve an incident power nearing 20 000 μmolPhotonPAR/m^2/s, *i.e.*, ten times the sun power midday midsummer.

6. Conclusion, limitations, and perspective

Taking a step back, this numerical investigation has shown that designing a super-high-light photobioreactor able to reproduce the light pattern required for *Chlorella vulgaris* to grow in such conditions seems achievable. Leveraging operational parameters and geometry adjustment, the median cycle frequency and the median duty cycle can be modulated. The design space explored in this work led to a frequency between 0.322 ± 0.065 and 0.625 ± 0.131 Hz, and a duty cycle between 0.200 ± 0.065 and 0.430 ± 0.110. Yet, they do not represent the extrema of the possible conditions, and future work is needed to complement these first steps.

Still, one should keep in mind that, before fine-tuning light/dark cycle patterns, it is essential to link them to the investigated biological outcomes (e.g., growth rate, pigment content, …). The same applies to the effects of temperature fluctuations within the photobioreactor. Furthermore, the light and temperature also have to be considered in conjunction, as they jointly shape the biological response [88]. This is all the more important because super high light can easily lead to photodamage or heat-induced damage, with recovery times extending one hour. This challenge is further exacerbated by the fact that existing models of flashing-light responses have generally been developed under conventional illumination conditions, while thermal models do not account for transient effects. Therefore, dedicated lab-scale experimental work is needed to generate the data required to address these limitations.

Finally, the perspective of future work also calls for the acknowledgment of a limitation of the hydrodynamic part of the proposed workflow. Indeed, as it relies on an Euler–Lagrange paradigm, it will not be able to predict some hydrodynamic phenomena, such as gas pockets, that may appear at higher aeration rates. This gas flooding of the photobioreactor would represent a limit, which could be bypassed using techniques developed by other scholars, such as using impellers to set the fluid into motion in the channel, also to be explored. In addition to working on the median values of the light cycle parameters, fine-tuning the flow to prevent the appearance of counterrotating vortices would also greatly benefit the system by distributing these parameters in an even narrower fashion and improving cooling efficiency. Overall, it can be concluded that realizing a super-high-light photobioreactor allowing to cultivate *Chlorella vulgaris* under 20 000 μmolPhotonPAR/m^2/s (ten times the sun power midday midsummer) is within reach and calling for the funding of an experimental validation.

Declaration of competing interest

The authors declare that they have no known competing financial interests or personal relationships that could have appeared to influence the work reported in this paper.

Acknowledgments

Communauté urbaine du Grand Reims, Département de la Marne, Région Grand Est and European Union (FEDER Grand Est 2021–2027) are acknowledged for their financial support to the Chair of Biotechnology of CentraleSupélec and the Centre Européen de Biotechnologie et de Bioéconomie (CEBB). Rishikesh Mishra is deeply thanked for having introduced the concept of Lagrangian Coherent Structures to the author. This work was supported by the French National Research Agency (ANR) under Grant No. ANR-26-ERCC-0007-01 (MEGASUN project).

Appendix A. Supplementary data

Supplementary material related to this article can be found online at https://doi.org/10.1016/j.algal.2026.104955.

Data availability

No data was used for the research described in the article.

References

[1] J.A. Garrido-Cardenas, F. Manzano-Agugliaro, F.G. Acien-Fernandez, E. Molina-Grima, Microalgae research worldwide, Algal Res. 35 (2018) 50–60, http://dx.doi.org/10.1016/j.algal.2018.08.005, URL https://www.sciencedirect.com/science/article/pii/S2211926418303436.

[2] M.S. Madeira, C. Cardoso, P.A. Lopes, D. Coelho, C. Afonso, N.M. Bandarra, J.A.M. Prates, Microalgae as feed ingredients for livestock production and meat quality: A review, Livest. Sci. 205 (2017) 111–121, http://dx.doi.org/10.1016/j.livsci.2017.09.020, URL https://www.sciencedirect.com/science/article/pii/S1871141317302858.

[3] W. Levasseur, P. Perré, V. Pozzobon, A review of high value-added molecules production by microalgae in light of the classification, Biotech. Adv. 41 (2020) 107545, http://dx.doi.org/10.1016/j.biotechadv.2020.107545, URL http://www.sciencedirect.com/science/article/pii/S0734975020300422.

[4] M. Rizwan, G. Mujtaba, S.A. Memon, K. Lee, N. Rashid, Exploring the potential of microalgae for new biotechnology applications and beyond: A review, Renew. Sustain. Energy Rev. 92 (2018) 394–404, http://dx.doi.org/10.1016/j.rser.2018.04.034, URL http://www.sciencedirect.com/science/article/pii/S1364032118302557.

[5] H. Chen, Q. Wang, Microalgae-based nitrogen bioremediation, Algal Res. 46 (2020) 101775, http://dx.doi.org/10.1016/j.algal.2019.101775, URL https://www.sciencedirect.com/science/article/pii/S2211926419311233.

[6] V. Pozzobon, N. Cui, A. Moreaud, E. Michiels, W. Levasseur, Nitrate and nitrite as mixed source of nitrogen for Chlorella vulgaris: Growth, nitrogen uptake and pigment contents, Bioresour. Technol. (2021) 124995, http://dx.doi.org/10.1016/j.biortech.2021.124995, URL https://www.sciencedirect.com/science/article/pii/S0960852421003345.

[7] M.K. Enamala, S. Enamala, M. Chavali, J. Donepudi, R. Yadavalli, B. Kolapalli, T.V. Aradhyula, J. Velpuri, C. Kuppam, Production of biofuels from microalgae - a review on cultivation, harvesting, lipid extraction, and numerous applications of microalgae, Renew. Sustain. Energy Rev. 94 (2018) 49–68, http://dx.doi.org/10.1016/j.rser.2018.05.012, URL http://www.sciencedirect.com/science/article/pii/S1364032118303551.

[8] S. Díaz, J. Settele, E. Brondizio, H.T. Ngo, M. Guèze, J. Agard, C. Zayas, Ipbes global assessment: summary for policymakers, 2019, Retrieved from IPBES website: https://www.ipbes.net/news/ipbes-global.

[9] R.H. Eckel, S.M. Grundy, P.Z. Zimmet, The metabolic syndrome, Lancet 365 (9468) (2005) 1415–1428, http://dx.doi.org/10.1016/S0140-6736(05)66378-7, URL https://www.sciencedirect.com/science/article/pii/S0140673605663787.

[10] J.P. Díaz, C. Inostroza, F.G. Acién, Scale-up of a Fibonacci-type photobioreactor for the production of Dunaliella salina, Appl. Biochem. Biotechnol. 193 (1) (2021) 188–204, http://dx.doi.org/10.1007/s12010-020-03410-x.

[11] I. Gifuni, A. Pollio, A. Marzocchella, G. Olivieri, New ultra-flat photobioreactor for intensive microalgal production: The effect of light irradiance, Algal Res. 34 (2018) 134–142, http://dx.doi.org/10.1016/j.algal.2018.07.014, URL http://www.sciencedirect.com/science/article/pii/S2211926417309839.

[12] A. Haydar, Photobioréacteur De Type Colonne À Bulles Confinée : Hydrodynamique, Transfert Gaz-Liquide, Influence Des Bulles Sur Le Cisaillement Pariétal Et Performances De Production (These de doctorat), Nantes Université, 2023, URL https://theses.fr/2023NANU4075.

[13] J. Masojídek, J. Kopecký, L. Giannelli, G. Torzillo, Productivity correlated to photobiochemical performance of chlorella mass cultures grown outdoors in thin-layer cascades, J. Ind. Microbiol. Biotechnol. 38 (2) (2011) 307–317, http://dx.doi.org/10.1007/s10295-010-0774-x.

[14] J. Pruvost, F. Le Borgne, A. Artu, J. Legrand, Development of a thin-film solar photobioreactor with high biomass volumetric productivity (AlgoFilm©) based on process intensification principles, Algal Res. 21 (2017) 120–137, http://dx.doi.org/10.1016/j.algal.2016.10.012, URL https://www.sciencedirect.com/science/article/pii/S2211926416305483.

[15] J.-F. Cornet, Calculation of optimal design and ideal productivities of volumetrically lightened photobioreactors using the constructal approach, Chem. Eng. Sci. 65 (2) (2010) 985–998, http://dx.doi.org/10.1016/j.ces.2009.09.052, URL https://www.sciencedirect.com/science/article/pii/S0009250909006551.

[16] J.H. de Vree, R. Bosma, M. Janssen, M.J. Barbosa, R.H. Wijffels, Comparison of four outdoor pilot-scale photobioreactors, Biotechnol. Biofuels 8 (1) (2015) 215, http://dx.doi.org/10.1186/s13068-015-0400-2.

[17] L. Straka, B.E. Rittmann, Dynamic response of synechocystis sp. PCC 6803 to changes in light intensity, Algal Res. 32 (2018) 210–220, http://dx.doi.org/10.1016/j.algal.2018.04.004, URL http://www.sciencedirect.com/science/article/pii/S2211926417302266.

[18] M.J. Griffiths, C. Garcin, R.P. van Hille, S.T.L. Harrison, Interference by pigment in the estimation of microalgal biomass concentration by optical density, J. Microbiol. Meth. 85 (2) (2011) 119–123, http://dx.doi.org/10.1016/j.mimet.2011.02.005, URL http://www.sciencedirect.com/science/article/pii/S016770121100056X.

[19] W. Levasseur, B. Taidi, R. Lacombe, P. Perré, V. Pozzobon, Impact of seconds to minutes photoperiods on Chlorella vulgaris growth rate and chlorophyll a and b content, Algal Res. 36 (2018) 10–16, http://dx.doi.org/10.1016/j.algal.2018.10.007.

[20] S.-H. Ho, S.-W. Huang, C.-Y. Chen, T. Hasunuma, A. Kondo, J.-S. Chang, Characterization and optimization of carbohydrate production from an indigenous microalga Chlorella vulgaris FSP-E, Bioresour. Technol. 135 (2013) 157–165, http://dx.doi.org/10.1016/j.biortech.2012.10.100, URL https://www.sciencedirect.com/science/article/pii/S0960852412016021.

[21] P.J. Janknegt, C.M.D. Graaff, W.H.V.D. Poll, R.J.W. Visser, J.W. Rijstenbil, A.G.J. Buma, Short-term antioxidative responses of 15 microalgae exposed to excessive irradiance including ultraviolet radiation, Eur. J. Phycol. 44 (4) (2009) 525–539, http://dx.doi.org/10.1080/09670260902943273.

[22] E.-M. Aro, I. Virgin, B. Andersson, Photoinhibition of photosystem II. inactivation, protein damage and turnover, Biochim. Biophys. Acta (BBA) - Bioenerg. 1143 (2) (1993) 113–134, http://dx.doi.org/10.1016/0005-2728(93)90134-2, URL https://www.sciencedirect.com/science/article/pii/0005272893901342.

[23] I. Ohad, N. Adir, H. Koike, D.J. Kyle, Y. Inoue, Mechanism of photoinhibition in vivo. A reversible light-induced conformational change of reaction center II is related to an irreversible modification of the D1 protein, J. Biol. Chem. 265 (4) (1990) 1972–1979, http://dx.doi.org/10.1016/S0021-9258(19)39927-2, URL https://www.sciencedirect.com/science/article/pii/S0021925819399272.

[24] I. Kedem, Y. Milrad, A. Kaplan, I. Yacoby, Juggling lightning: How Chlorella ohadii handles extreme energy inputs without damage, Photosynth. Res. 147 (3) (2021) 329–344, http://dx.doi.org/10.1007/s11120-020-00809-9.

[25] J. Masojidek, S. Papacek, M. Sergejevova, V. Jirka, J. Cerveny, J. Kunc, J. Korecko, O. Verbovikova, J. Kopecky, D. Stys, G. Torzillo, A closed solar photobioreactor for cultivation of microalgae under supra-high irradiance: basic design and performance, J. Appl. Phycol. 15 (2) (2003) 239–248, http://dx.doi.org/10.1023/A:1023849117102.

[26] H. Qiang, Y. Zarmi, A. Richmond, Combined effects of light intensity, light-path and culture density on output rate of Spirulina platensis (Cyanobacteria), Eur. J. Phycol. 33 (2) (1998) 165–171, URL https://www.cambridge.org/core/journals/european-journal-of-phycology/article/combined-effects-of-light-intensity-lightpath-and-culture-density-on-output-rate-of-spirulina-platensis-cyanobacteria/1DA433EAEFFBAA39DA9F88F5F7EF70EC.

[27] V. Pozzobon, Chlorella vulgaris cultivation under super high light intensity: An application of the flashing light effect, Algal Res. 68 (2022) 102874, http://dx.doi.org/10.1016/j.algal.2022.102874, URL https://www.sciencedirect.com/science/article/pii/S2211926422002454.

[28] J.N. Phillips, J. Myers, Growth rate of Chlorella in flashing light. 1, Plant Physiol. 29 (2) (1954) 152–161, URL https://www.ncbi.nlm.nih.gov/pmc/articles/PMC540481/.

[29] B. Kok, Chapter 6, in: Algal Culture from Laboratory To Pilot Plant, Carnegie Institute Washington Pub, 1953, pp. 63–75.

[30] S. Abu-Ghosh, D. Fixler, Z. Dubinsky, D. Iluz, Flashing light in microalgae biotechnology, Bioresour. Technol. 203 (2016) 357–363, http://dx.doi.org/10.1016/j.biortech.2015.12.057, URL http://www.sciencedirect.com/science/article/pii/S0960852415016879.

[31] P.S.C. Schulze, R. Guerra, H. Pereira, L.M. Schüler, J.C.S. Varela, Flashing LEDs for microalgal production, Trends Biotechnol. 35 (11) (2017) 1088–1101, http://dx.doi.org/10.1016/j.tibtech.2017.07.011, URL http://www.sciencedirect.com/science/article/pii/S0167779917301919.

[32] J.U. Grobbelaar, L. Nedbal, V. Tichý, Influence of high frequency light/dark fluctuations on photosynthetic characteristics of microalgae photoacclimated to different light intensities and implications for mass algal cultivation, J. Appl. Phycol. 8 (4) (1996) 335–343, http://dx.doi.org/10.1007/BF02178576.

[33] M.J. Barbosa, M. Janssen, N. Ham, J. Tramper, R.H. Wijffels, Microalgae cultivation in air-lift reactors: Modeling biomass yield and growth rate as a function of mixing frequency, Biotechnol. Bioeng. 82 (2) (2003) 170–179, http://dx.doi.org/10.1002/bit.10563, _eprint: https://onlinelibrary.wiley.com/doi/pdf/10.1002/bit.10563. URL https://onlinelibrary.wiley.com/doi/abs/10.1002/bit.10563.

[34] J. Yarnold, I.L. Ross, B. Hankamer, Photoacclimation and productivity of Chlamydomonas reinhardtii grown in fluctuating light regimes which simulate outdoor algal culture conditions, Algal Res. 13 (2016) 182–194, http://dx.doi.org/10.1016/j.algal.2015.11.001, URL https://www.sciencedirect.com/science/article/pii/S2211926415300928.

[35] M. Bonnanfant, B. Jesus, J. Pruvost, J.-L. Mouget, D.A. Campbell, Photosynthetic electron transport transients in Chlorella vulgaris under fluctuating light, Algal Res. 44 (2019) 101713, http://dx.doi.org/10.1016/j.algal.2019.101713, URL https://www.sciencedirect.com/science/article/pii/S2211926419304400.

[36] L. Nedbal, V. Tichý, F. Xiong, J.U. Grobbelaar, Microscopic green algae and cyanobacteria in high-frequency intermittent light, J. Appl. Phycol. 8 (4) (1996) 325–333, http://dx.doi.org/10.1007/BF02178575.

[37] C. Vejrazka, M. Janssen, M. Streefland, R.H. Wijffels, Photosynthetic efficiency of chlamydomonas reinhardtii in flashing light, Biotechnol. Bioeng. 108 (12) (2011) 2905–2913, http://dx.doi.org/10.1002/bit.23270, _eprint: https://onlinelibrary.wiley.com/doi/pdf/10.1002/bit.23270. URL https://onlinelibrary.wiley.com/doi/abs/10.1002/bit.23270.

[38] C. Vejrazka, M. Janssen, G. Benvenuti, M. Streefland, R.H. Wijffels, Photosynthetic efficiency and oxygen evolution of Chlamydomonas reinhardtii under continuous and flashing light, Appl. Microbiol. Biotechnol. 97 (4) (2013) 1523–1532, http://dx.doi.org/10.1007/s00253-012-4390-8.

[39] A. Saccardo, A. Porcelli, L. Borella, E. Sforza, F. Bezzo, Model-based optimisation of microalgae growth under high-intensity and high-frequency pulsed light conditions, J. Clean. Prod. 469 (2024) 143238, http://dx.doi.org/10.1016/j.jclepro.2024.143238, URL https://www.sciencedirect.com/science/article/pii/S0959652624026878.

[40] Y. Zarmi, J.M. Gordon, A. Mahulkar, A.R. Khopkar, S.D. Patil, A. Banerjee, B.G. Reddy, T.P. Griffin, A. Sapre, Enhanced Algal photosynthetic photon efficiency by pulsed light, IScience 23 (5) (2020) 101115, http://dx.doi.org/10.1016/j.isci.2020.101115, URL https://www.sciencedirect.com/science/article/pii/S258900422030300X.

[41] G. Steiner, D. Saini, C. Gates, Extreme light acclimation reveals inherent photoprotective mechanisms in a natively low-light *Chlorella*, Algal Res. 96 (2026) 104727, http://dx.doi.org/10.1016/j.algal.2026.104727, URL https://www.sciencedirect.com/science/article/pii/S2211926426002122.

[42] P. Hartmann, D. Demory, C. Combe, R. Hamouda, A.-C. Boulanger, M.-O. Bristeau, J. Sainte-Marie, B. Sialve, J.-P. Steyer, S. Rabouille, A. Sciandra, O. Bernard, Growth rate estimation of algae in raceway ponds: A novel approach, IFAC Proc. Vol. 47 (3) (2014) 6216–6221, http://dx.doi.org/10.3182/20140824-6-ZA-1003.02408, URL http://www.sciencedirect.com/science/article/pii/S1474667016425863.

[43] K. Liffman, D.A. Paterson, P. Liovic, P. Bandopadhayay, Comparing the energy efficiency of different high rate algal raceway pond designs using computational fluid dynamics, Chem. Eng. Res. Des. 91 (2) (2013) 221–226, http://dx.doi.org/10.1016/j.cherd.2012.08.007, URL https://www.sciencedirect.com/science/article/pii/S0263876212003048.

[44] L. Giannelli, H. Yamaji, T. Katsuda, A numerical model for the quantification of light/dark cycles in microalgal cultures: Air-lift and bubble-column photobioreactor analysis by means of computational fluid dynamics, J. Chem. Eng. Jpn. 48 (1) (2015) 61–71, http://dx.doi.org/10.1252/jcej.14we093, URL https://www.jstage.jst.go.jp/article/jcej/48/1/48_14we093/_article/-char/ja/.

[45] M.R. Rampure, A.A. Kulkarni, V.V. Ranade, Hydrodynamics of bubble column reactors at high gas velocity: Experiments and computational fluid dynamics (CFD) simulations, Ind. Eng. Chem. Res. 46 (25) (2007) 8431–8447, http://dx.doi.org/10.1021/ie070079h.

[46] I. Perner-Nochta, C. Posten, Simulations of light intensity variation in photobioreactors, J. Biotech. 131 (3) (2007) 276–285, http://dx.doi.org/10.1016/j.jbiotec.2007.05.024, URL http://www.sciencedirect.com/science/article/pii/S0168165607003720.

[47] C. Qin, J. Wu, J. Wang, Synergy between flow and light fields and its applications to the design of mixers in microalgal photobioreactors, Biotechnol. Biofuels 12 (1) (2019) 93, http://dx.doi.org/10.1186/s13068-019-1430-y.

[48] X. Gao, B. Kong, R. Dennis Vigil, Comprehensive computational model for combining fluid hydrodynamics, light transport and biomass growth in a Taylor vortex algal photobioreactor: Eulerian approach, Algal Res. 24 (2017) 1–8, http://dx.doi.org/10.1016/j.algal.2017.03.009, URL https://www.sciencedirect.com/science/article/pii/S2211926416303563.

[49] J. Huang, F. Feng, M. Wan, J. Ying, Y. Li, X. Qu, R. Pan, G. Shen, W. Li, Improving performance of flat-plate photobioreactors by installation of novel internal mixers optimized with computational fluid dynamics, Bioresour. Technol. 182 (2015) 151–159, http://dx.doi.org/10.1016/j.biortech.2015.01.067, URL https://www.sciencedirect.com/science/article/pii/S0960852415000875.

[50] T. Sato, D. Yamada, S. Hirabayashi, Development of virtual photobioreactor for microalgae culture considering turbulent flow and flashing light effect, Energy Convers. Manage. 51 (6) (2010) 1196–1201, http://dx.doi.org/10.1016/j.enconman.2009.12.030, URL http://www.sciencedirect.com/science/article/pii/S0196890409005366.

[51] X. Gao, B. Kong, R.D. Vigil, Simulation of algal photobioreactors: recent developments and challenges, Biotechnol. Lett. 40 (9) (2018) 1311–1327, http://dx.doi.org/10.1007/s10529-018-2595-3.

[52] G. Haller, Lagrangian coherent structures from approximate velocity data, Phys. Fluids 14 (6) (2002) 1851–1861, http://dx.doi.org/10.1063/1.1477449, URL https://pubs.aip.org/aip/pof/article/14/6/1851/254733/Lagrangian-coherent-structures-from-approximate.

[53] S. Gao, S. Edmundson, M. Huesemann, Oxygen stress mitigation for microalgal biomass productivity improvement in outdoor raceway ponds, Algal Res. 68 (2022) 102901, http://dx.doi.org/10.1016/j.algal.2022.102901, URL https://www.sciencedirect.com/science/article/pii/S2211926422002727.

[54] E. Posadas, M.d.M. Morales, C. Gomez, F.G. Acién, R. Muñoz, Influence of pH and CO2 source on the performance of microalgae-based secondary domestic wastewater treatment in outdoors pilot raceways, Chem. Eng. J. 265 (2015) 239–248, http://dx.doi.org/10.1016/j.cej.2014.12.059, URL https://www.sciencedirect.com/science/article/pii/S1385894714016738.

[55] J. Degen, A. Uebele, A. Retze, U. Schmid-Staiger, W. Trösch, A novel airlift photobioreactor with baffles for improved light utilization through the flashing light effect, J. Biotech. 92 (2) (2001) 89–94, http://dx.doi.org/10.1016/S0168-1656(01)00350-9, URL https://www.sciencedirect.com/science/article/pii/S0168165601003509.

[56] V. Pozzobon, Impact of bubbles on the light field within a photobioreactor: A practical design tool, Algal Res. 91 (2025) 104331, http://dx.doi.org/10.1016/j.algal.2025.104331, URL https://www.sciencedirect.com/science/article/pii/S2211926425004424.

[57] R. Kandilian, A. Soulies, J. Pruvost, B. Rousseau, J. Legrand, L. Pilon, Simple method for measuring the spectral absorption cross-section of microalgae, Chem. Eng. Sci. 146 (2016) 357–368, http://dx.doi.org/10.1016/j.ces.2016.02.039, URL https://www.sciencedirect.com/science/article/pii/S0009250916300938.

[58] B. Baránková, D. Lazár, J. Nauš, A. Solovchenko, O. Gorelova, O. Baulina, G. Huber, L. Nedbal, Light absorption and scattering by high light-tolerant, fast-growing Chlorella vulgaris IPPAS C-1 cells, Algal Res. 49 (2020) 101881, http://dx.doi.org/10.1016/j.algal.2020.101881, URL https://www.sciencedirect.com/science/article/pii/S2211926419310963.

[59] L.A. Castillo, P.J. Valadés-Pelayo, H.J. Avila-Paredes, J.J. Cabello, A. Balbuena, Methodology for the fast direct estimation of spectral radiative transport properties in microalgae photobioreactors, Chem. Eng. J. 458 (2023) 141462, http://dx.doi.org/10.1016/j.cej.2023.141462, URL https://www.sciencedirect.com/science/article/pii/S1385894723001936.

[60] W. Levasseur, P. Perré, V. Pozzobon, Chlorella vulgaris acclimated cultivation under flashing light: An in-depth investigation under iso-actinic conditions, Algal Res. 70 (2023) 102976, http://dx.doi.org/10.1016/j.algal.2023.102976, URL https://www.sciencedirect.com/science/article/pii/S2211926423000097.

[61] N. Usui, M. Ikenouchi, The biological CO2 fixation and utilization project by RITE(1) — Highly-effective photobioreactor system, Energy Convers. Manage. 38 (1997) S487–S492, http://dx.doi.org/10.1016/S0196-8904(96)00315-9, URL https://www.sciencedirect.com/science/article/pii/S0196890496003159.

[62] T. Smalley, F.J. Fields, A.J.E. Berndt, J.T. Ostrand, V. Heredia, S.P. Mayfield, Improving biomass and lipid yields of Desmodesmus armatus and Chlorella vulgaris through mutagenesis and high-throughput screening, Biomass Bioenergy 142 (2020) 105755, http://dx.doi.org/10.1016/j.biombioe.2020.105755, URL http://www.sciencedirect.com/science/article/pii/S0961953420302890.

[63] J. Yin, W. Levasseur, V. Pozzobon, Temperature effects on growth and biochemical composition of *Chlorella vulgaris* under heterotrophic cultivation, Plant Physiol. Biochem. 236 (2026) 111431, http://dx.doi.org/10.1016/j.plaphy.2026.111431, URL https://www.sciencedirect.com/science/article/pii/S0981942826004171.

[64] W. Jiang, W. Levasseur, J. Casalinho, T. Martin, F. Puel, P. Perré, V. Pozzobon, Shear stress computation in a millimeter thin flat panel photobioreactor: Numerical design validated by experiments, Biotechnol. Appl. Biochem. 68 (1) (2021) 60–70, http://dx.doi.org/10.1002/bab.1894, _eprint: https://iubmb.onlinelibrary.wiley.com/doi/pdf/10.1002/bab.1894. URL https://iubmb.onlinelibrary.wiley.com/doi/abs/10.1002/bab.1894.

[65] C. McHardy, G. Luzi, C. Lindenberger, J.R. Agudo, A. Delgado, C. Rauh, Numerical analysis of the effects of air on light distribution in a bubble column photobioreactor, Algal Res. 31 (2018) 311–325, http://dx.doi.org/10.1016/j.algal.2018.02.016, URL https://www.sciencedirect.com/science/article/pii/S2211926417309426.

[66] H. Wang, J. Liu, Z. Guo, K. Takahashi, Non-Fourier heat conduction study for steady states in metallic nanofilms, Chin. Sci. Bull. 57 (24) (2012) 3239–3243, http://dx.doi.org/10.1007/s11434-012-5288-7.

[67] V. Pozzobon, P. Perré, Multiscale numerical workflow describing microalgae motion and light pattern incidence towards population growth in a photobioreactor, J. Theoret. Biol. 498 (2020) 110293, http://dx.doi.org/10.1016/j.jtbi.2020.110293, URL https://www.sciencedirect.com/science/article/pii/S002251932030148X.

[68] X. Zhang, Z. Jiang, L. Chen, A. Chou, H. Yan, Y.Y. Zuo, X. Zhang, Influence of cell properties on rheological characterization of microalgae suspensions, Bioresour. Technol. 139 (2013) 209–213, http://dx.doi.org/10.1016/j.biortech.2013.03.195, URL https://www.sciencedirect.com/science/article/pii/S0960852413005993.

[69] A. Cartellier, M. Andreotti, P. Sechet, Induced agitation in homogeneous bubbly flows at moderate particle Reynolds number, Phys. Rev. E 80 (6) (2009) 065301, http://dx.doi.org/10.1103/PhysRevE.80.065301, URL https://link.aps.org/doi/10.1103/PhysRevE.80.065301.

[70] F. Fasaei, J.H. Bitter, P.M. Slegers, A.J.B. van Boxtel, Techno-economic evaluation of microalgae harvesting and dewatering systems, Algal Res. 31 (2018) 347–362, http://dx.doi.org/10.1016/j.algal.2017.11.038, URL http://www.sciencedirect.com/science/article/pii/S2211926417306677.

[71] J.-C. Shyu, C.-W. Chang, P.-H. Chen, A simplified correlation for bubble volume estimation, Can. J. Chem. Eng. 84 (2) (2006) 183–188, http://dx.doi.org/10.1002/cjce.5450840205, _eprint: https://onlinelibrary.wiley.com/doi/pdf/10.1002/cjce.5450840205. URL https://onlinelibrary.wiley.com/doi/abs/10.1002/cjce.5450840205.

[72] T.L. Bergman, A.S. Lavine, F.P. Incropera, D.P. DeWitt, Fundamentals of Heat and Mass Transfer, 8th Edition, eighth ed., Wiley, 2017.

[73] A. Bar-Cohen, W.M. Rohsenow, Thermally optimum spacing of vertical, natural convection cooled, parallel plates, J. Heat Transf. 106 (1) (1984) 116–123, http://dx.doi.org/10.1115/1.3246622.

[74] V. Gnielinski, Neue Gleichungen für den Wärme- und den Stoffübergang in turbulent durchströmten Rohren und Kanälen, Forsch. Ingenieurwesen A 41 (1) (1975) 8–16, http://dx.doi.org/10.1007/BF02559682.

[75] H. Jasak, A. Jemcov, Z. Tukovic, OpenFOAM: A C++ library for complex physics simulations, in: International Workshop on Coupled Methods in Numerical Dynamics, Vol. 1000, Dubrovnik, Croatia), 2007, pp. 1–20.

[76] C. Habes, A.v. Kameke, M.E. Fadeli, H. Marschall, Lcs4foam – an OpenFOAM function object to compute Lagrangian coherent structures, OpenFOAM® J. 4 (2024) 118–131, http://dx.doi.org/10.51560/ofj.v4.141, URL https://journal.openfoam.com/index.php/ofj/article/view/141.

[77] J.G. Baker, J.R. van Meter, Reducing reflections from mesh refinement interfaces in numerical relativity, Phys. Rev. D 72 (10) (2005) 104010, http://dx.doi.org/10.1103/PhysRevD.72.104010, URL https://link.aps.org/doi/10.1103/PhysRevD.72.104010.

[78] I.B. Celik, U. Ghia, P.J. Roache, C.J. Freitas, Procedure for estimation and reporting of uncertainty due to discretization in CFD applications, J. Fluids Eng.-Trans. ASME 130 (7) (2008)

[79] P.J. Roache, Perspective: A method for uniform reporting of grid refinement studies, J. Fluids Eng. 116 (3) (1994) 405–413, http://dx.doi.org/10.1115/1.2910291.

[80] Y. Shirian, J.A.K. Horwitz, A. Mani, On the convergence of statistics in simulations of stationary incompressible turbulent flows, Comput. & Fluids 266 (2023) 106046, http://dx.doi.org/10.1016/j.compfluid.2023.106046, URL https://www.sciencedirect.com/science/article/pii/S0045793023002712.

[81] J. Sucec, Exact Analytical Solution to a Transient Conjugate Heat-Transfer Problem, Tech. Rep. E-7090, 1973, NTRS Author Affiliations: NASA Lewis Research Center NTRS Document ID: 19730007228 NTRS Research Center: Legacy CDMS (CDMS). URL https://ntrs.nasa.gov/citations/19730007228?utm_source=chatgpt.com.

[82] M. Rebej, T. Juřena, J. Vondál, D. Fuente Herraiz, J. Červený, Z. Jegla, Numerical simulations and validation of single- and two-phase flow in a stirred lab-scale photobioreactor, Biosyst. Eng. 230 (2023) 35–50, http://dx.doi.org/10.1016/j.biosystemseng.2023.04.004, URL https://www.sciencedirect.com/science/article/pii/S153751102300079X.

[83] S.Y. Liew, Z.Y. Lam, J. Gimbun, Experimental measurement and CFD simulation on the hydrodynamics of an internal-loop airlift reactor, MATEC Web Conf. 111 (2017) 01002, http://dx.doi.org/10.1051/matecconf/201711101002, URL https://www.matec-conferences.org/articles/matecconf/abs/2017/25/matecconf_fluid2017_01002/matecconf_fluid2017_01002.html.

[84] S. Qie, F. Gao, C. Liu, Z. Huang, C. Liu, Effects of different draft baffles on the hydrodynamics in internal-loop airlift reactors, Trans. Tianjin Univ. 21 (5) (2015) 446–452, http://dx.doi.org/10.1007/s12209-015-2513-x.

[85] W. Trösch, U. Schmid-Staiger, A. Zastrow, A. Retze, F. Brucker, Photobioreactor with improved supply of light by surface enlargement, wavelength shifter bars or light transport, 2003, URL https://patents.google.com/patent/US6509188B1/en.

[86] M. Bonnanfant, H. Marec, B. Jesus, J.-L. Mouget, J. Pruvost, Investigation of the photosynthetic response of Chlorella vulgaris to light changes in a torus-shape photobioreactor, Appl. Microbiol. Biotechnol. 105 (23) (2021) 8689–8701, http://dx.doi.org/10.1007/s00253-021-11636-w.

[87] E. Bellos, P. Lykas, C. Tzivanidis, Heat and flow study of the internally finned tubes with different fin geometries, Appl. Syst. Innov. 5 (3) (2022) 50, http://dx.doi.org/10.3390/asi5030050, URL https://www.mdpi.com/2571-5577/5/3/50.

[88] C. Sorokin, R.W. Krauss, Effects of temperature & illuminance on chlorella growth uncoupled from cell division, Plant Physiol. 37 (1) (1962) 37–42, URL https://www.ncbi.nlm.nih.gov/pmc/articles/PMC549734/.